MAELAS: MAgneto-ELAStic properties calculation via computational high-throughput approach

P. Nieves[a,*], S. Arapan[a], S. H. Zhang[b,c], A. P. Kądzielawa[a], R. F. Zhang[b,c], D. Legut[a]

[a]*IT4Innovations, VŠB - Technical University of Ostrava, 17. listopadu 2172/15, 70800 Ostrava-Poruba, Czech Republic*
[b]*School of Materials Science and Engineering, Beihang University, Beijing 100191, PR China*
[c]*Center for Integrated Computational Materials Engineering, International Research Institute for Multidisciplinary Science, Beihang University, Beijing 100191, PR China*

Abstract

In this work, we present the program MAELAS to calculate magnetocrystalline anisotropy energy, anisotropic magnetostrictive coefficients and magnetoelastic constants in an automated way by Density Functional Theory calculations. The program is based on the length optimization of the unit cell proposed by Wu and Freeman to calculate the magnetostrictive coefficients for cubic crystals. In addition to cubic crystals, this method is also implemented and generalized for other types of crystals that may be of interest in the study of magnetostrictive materials. As a benchmark, some tests are shown for well-known magnetic materials.

PROGRAM SUMMARY
Program Title: MAELAS
Developer's respository link: https://github.com/pnieves2019/MAELAS
Licensing provisions: BSD 3-clause
Programming language: Python3
Nature of problem: To calculate anisotropic magnetostrictive coefficients and magnetoelastic constants in an automated way based on Density Functional Theory methods.
Solution method: In the first stage, the unit cell is relaxed through a spin-polarized cal-

---

*Corresponding author.
E-mail address:* pablo.nieves.cordones@vsb.cz

culation without SOC. Next, after a crystal symmetry analysis, a set of deformed lattice and spin configurations are generated using the pymatgen library [1]. The energy of these states is calculated by the first-principles code VASP [3], including the SOC. The anisotropic magnetostrictive coefficients are derived from the fitting of these energies to a quadratic polynomial [2]. Finally, if the elastic tensor is provided [4], then the magnetoelastic constants are calculated too.

Additional comments including restrictions and unusual features: This version supports the following crystal systems: Cubic (point groups 432, $\bar{4}3m$, $m\bar{3}m$), Hexagonal (6mm, 622, $\bar{6}2m$, 6/mmm), Trigonal (32, 3m, $\bar{3}m$), Tetragonal (4mm, 422, $\bar{4}2m$, 4/mmm) and Orthorhombic (222, 2mm, mmm).

References

[1] S. P. Ong, W. D. Richards, A. Jain, G. Hautier, M. Kocher, S. Cholia, D. Gunter, V. L. Chevrier, K. A. Persson, and G. Ceder, Comput. Mater. Sci. 68, 314 (2013).

[2] R. Wu, A. J. Freeman, Journal of Applied Physics 79, 6209–6212 (1996).

[3] G. Kresse, J. Furthmüller, Phys. Rev. B 54 (1996) 11169.

[4] S. Zhang and R. Zhang, Comput. Phys. Commun. 220, 403 (2017).

1. Introduction

A magnetostrictive material is one which changes in size due to a change of state of magnetization. These materials are characterized by magnetostrictive coefficients (λ). In many technical applications such as electric transformers, motor shielding, and magnetic recording, magnetic materials with extremely small magnetostrictive coefficients are required. By contrast, materials with large magnetostrictive coefficients are needed for many applications in electromagnetic microdevices as actuators and sensors [1–4]. Typically, elementary Rare-Earth (R) metals (under low temperature and high magnetic field) and compounds with R and transition metals exhibit a high magnetostriction ($\lambda > 10^{-3}$). In particular, the highest magnetostrictions were found in the RFe_2 compounds with Laves phase C15 structure type (face centered cubic) [5]. For instance, Terfenol-D ($Tb_{0.27}Dy_{0.73}Fe_2$) is a widely used magnetostrictive material thanks to its giant magnetostriction along [111] crystallographic direction ($\lambda_{111} = 1.6 \times 10^{-3}$) under moderate magnetic fields (< 2 kOe) at room temperature [6]. Beyond cubic

systems, the research of magnetostrictive materials has been focused on hexagonal crystals like RCo_5 (space group 191), hexagonal and trigonal R_2Co_7 and R_2Co_{17} series, and tetragonal $R_2Fe_{14}B$ [7, 8]. More recently, the problem of R availability [9] has also motivated the exploration of R-free magnetostrictive materials like Galfenol (Fe-Ga), spinel ferrites ($CoFe_2O_4$), Nitinol (Ni-Ti alloys), Fe-based Invars, and Ni_2MnGa [10–12].

Concerning the theory of magnetostriction, the basic equations for cubic (I) crystals were developed by Akulov [13] and Becker et al. [14] in the 1920s and 30s. In the next three decades, great advances took place due to the outstanding works of Mason [15], Clark et al. [16], and Callen and Callen [17], as well as many others, where the theory was extended to other crystal symmetries. Over the last decades, modern electronic structure theory based on Density Functional Theory (DFT) has been successfully applied to describe magnetostriction of many materials [1, 10, 11, 18–29]. Nowadays, a common method to calculate magnetostrictive coefficients is based on the optimization of the unit cell length proposed by Wu and Freeman for cubic crystals [18, 19]. In this work, we present the MAELAS program where this methodology is implemented and generalized for the main crystal symmetries in the research field of magnetostriction. The paper is organized as follows. In Section 2, we review some theoretical concepts and equations of magnetostriction. In Section 3, we explain in detail the methodology and workflow of the program, while some examples are shown in Section 4. The paper ends with a summary of the main conclusions and future perspectives (Section 5).

2. Theory of magnetostriction

The magnetostrictive response is mainly originated by two kind of sources: (i) isotropic exchange interaction and (ii) strain dependence of magnetocrystalline anisotropy [8]. The magnetostriction due to isotropic exchange leads to fractional volume changes, and doesn't depend on the magnetization direction [30]. On the other hand, the strain dependence of magnetocrystalline anisotropy is responsible for the magnetostriction that depends on the magnetization orientation (anisotropic), and is originated by the spin-orbit coupling (SOC) and crystal field interactions [8, 31]. The current version of the program MAELAS calculates the magnetostrictive coefficients and magnetoelastic constants related to the anisotropic magnetostriction.

Let's consider l_0 the initial length of a demagnetized material along the direction $\boldsymbol{\beta}$ ($|\boldsymbol{\beta}| = 1$), and l the final length along the same direction $\boldsymbol{\beta}$ when the
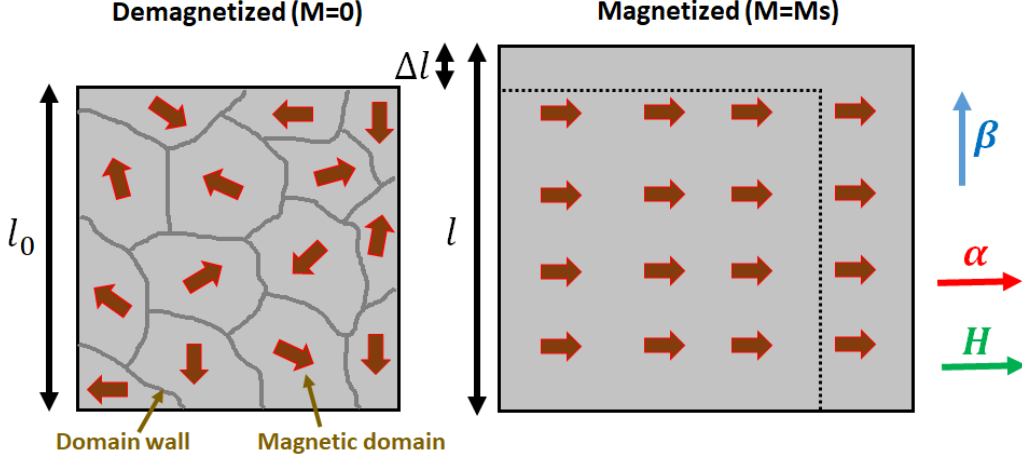
3

Figure 1: Magnetostriction of a single crystal under an external magnetic field ($\boldsymbol{\alpha}\|\boldsymbol{H}$) perpendicular to the measured length direction ($\boldsymbol{\beta}\perp\boldsymbol{H}$). Symbols M and M_s stand for macroscopic magnetization and saturation magnetization, respectively. Dash line on the right represents the original size of the demagnetized material. The magnetostriction effect has been magnified in order to help to visualize it easily, in real materials it is smaller ($\Delta l/l_0 \sim 10^{-3} - 10^{-6}$).

system is magnetized along the direction $\boldsymbol{\alpha}$ ($|\boldsymbol{\alpha}| = 1$). The relative length change $(l - l_0)/l_0 = \Delta l/l_0$ can be written as [8]

$$\left.\frac{\Delta l}{l_0}\right|_{\boldsymbol{\beta}}^{\boldsymbol{\alpha}} = \sum_{i,j=x,y,z} \varepsilon_{ij}^{eq}(\boldsymbol{\alpha})\beta_i\beta_j, \tag{1}$$

where ε_{ij}^{eq} is the equilibrium strain tensor. This equation describes the Joule effect [32], once it is rewritten in terms of the magnetostrictive coefficients (λ) conveniently. Fig.1 shows a sketch of magnetostriction.

The deformation of a solid can be described in terms of the displacement vector $\boldsymbol{u}(\boldsymbol{r}) = \boldsymbol{r}' - \boldsymbol{r}$ that gives the displacement of a point at the initial position $\boldsymbol{r}$ to its final position $\boldsymbol{r}'$ after it is deformed. For small deformations (infinitesimal strain theory), the strain tensor (ε_{ij}) can be expressed in terms of the displacement vector as[33]

$$\varepsilon_{ij} = \frac{1}{2}\left(\frac{\partial u_i}{\partial r_j} + \frac{\partial u_j}{\partial r_i}\right), \qquad i,j = x,y,z \tag{2}$$

where $\partial u_i/\partial r_j$ is called the displacement gradient (second-order tensor). The equilibrium strain tensor is obtained through the minimization of both the elastic (E_{el})

4

and magnetoelastic (E_{me}) energies [5, 8]

$$\frac{\partial(E_{el}+E_{me})}{\partial\varepsilon_{ij}} = 0, \qquad i,j = x,y,z \tag{3}$$

where the total energy must be invariant under the symmetry operations of the crystal lattice [5]. Let's write general equations for E_{el} and E_{me}. The elastic energy depends on the fourth-order elastic stiffness tensor c_{ijkl} that links the second-order strain and stress (σ_{ij}) tensors through the generalized Hooke's law

$$\sigma_{ij} = \sum_{k,l=x,y,z} c_{ijkl}\varepsilon_{kl}, \quad i,j = x,y,z. \tag{4}$$

Taking advantage of the symmetry of stress and strain tensors, the Hooke's law can be written in matrix notation as

$$\begin{pmatrix} \sigma_{xx} \\ \sigma_{yy} \\ \sigma_{zz} \\ \sigma_{yz} \\ \sigma_{xz} \\ \sigma_{xy} \end{pmatrix} = \begin{pmatrix} c_{xxxx} & c_{xxyy} & c_{xxzz} & c_{xxyz} & c_{xxzx} & c_{xxxy} \\ c_{yyxx} & c_{yyyy} & c_{yyzz} & c_{yyyz} & c_{yyzx} & c_{yyxy} \\ c_{zzxx} & c_{zzyy} & c_{zzzz} & c_{zzyz} & c_{zzzx} & c_{zzxy} \\ c_{yzxx} & c_{yzyy} & c_{yzzz} & c_{yzyz} & c_{yzzx} & c_{yzxy} \\ c_{zxxx} & c_{zxyy} & c_{zxzz} & c_{zxyz} & c_{zxzx} & c_{zxxy} \\ c_{xyxx} & c_{xyyy} & c_{xyzz} & c_{xyyz} & c_{xyzx} & c_{xyxy} \end{pmatrix} \begin{pmatrix} \varepsilon_{xx} \\ \varepsilon_{yy} \\ \varepsilon_{zz} \\ 2\varepsilon_{yz} \\ 2\varepsilon_{xz} \\ 2\varepsilon_{xy} \end{pmatrix} \tag{5}$$

To facilitate the manipulation of this equation it is convenient to define the following six-dimensional vectors (Voigt notation)

$$\tilde{\boldsymbol{\sigma}} = \begin{pmatrix} \tilde{\sigma}_1 \\ \tilde{\sigma}_2 \\ \tilde{\sigma}_3 \\ \tilde{\sigma}_4 \\ \tilde{\sigma}_5 \\ \tilde{\sigma}_6 \end{pmatrix} = \begin{pmatrix} \sigma_{xx} \\ \sigma_{yy} \\ \sigma_{zz} \\ \sigma_{yz} \\ \sigma_{xz} \\ \sigma_{xy} \end{pmatrix}, \qquad \tilde{\boldsymbol{\varepsilon}} = \begin{pmatrix} \tilde{\varepsilon}_1 \\ \tilde{\varepsilon}_2 \\ \tilde{\varepsilon}_3 \\ \tilde{\varepsilon}_4 \\ \tilde{\varepsilon}_5 \\ \tilde{\varepsilon}_6 \end{pmatrix} = \begin{pmatrix} \varepsilon_{xx} \\ \varepsilon_{yy} \\ \varepsilon_{zz} \\ 2\varepsilon_{yz} \\ 2\varepsilon_{xz} \\ 2\varepsilon_{xy} \end{pmatrix}, \tag{6}$$

and replace c_{ijkl} by C_{nm} contracting a pair of cartesian indices into a single integer: $xx \to 1$, $yy \to 2$, $zz \to 3$, $yz \to 4$, $xz \to 5$ and $xy \to 6$. Using these conversion rules the Hooke's law is simplified to

$$\tilde{\sigma}_i = \sum_{j=1}^{6} C_{ij}\tilde{\varepsilon}_j, \quad i = 1,...,6 \tag{7}$$

where in matrix form reads

$$
\begin{pmatrix} \tilde{\sigma}_1 \\ \tilde{\sigma}_2 \\ \tilde{\sigma}_3 \\ \tilde{\sigma}_4 \\ \tilde{\sigma}_5 \\ \tilde{\sigma}_6 \end{pmatrix} = \begin{pmatrix} C_{11} & C_{12} & C_{13} & C_{14} & C_{15} & C_{16} \\ C_{21} & C_{22} & C_{23} & C_{24} & C_{25} & C_{26} \\ C_{31} & C_{32} & C_{33} & C_{34} & C_{35} & C_{36} \\ C_{41} & C_{42} & C_{42} & C_{44} & C_{45} & C_{46} \\ C_{51} & C_{52} & C_{53} & C_{54} & C_{55} & C_{56} \\ C_{61} & C_{62} & C_{63} & C_{64} & C_{65} & C_{66} \end{pmatrix} \begin{pmatrix} \tilde{\varepsilon}_1 \\ \tilde{\varepsilon}_2 \\ \tilde{\varepsilon}_3 \\ \tilde{\varepsilon}_4 \\ \tilde{\varepsilon}_5 \\ \tilde{\varepsilon}_6 \end{pmatrix}. \tag{8}
$$

where $C_{ij} = C_{ji}$. Then the elastic energy up to second-order in the strain can be written as

$$
E_{el} = E_0 + \frac{V_0}{2} \sum_{i,j=1}^{6} C_{ij} \tilde{\varepsilon}_i \tilde{\varepsilon}_j + O(\tilde{\varepsilon}^3), \tag{9}
$$

where E_0 and V_0 are the equilibrium energy and volume, respectively. The magnetoelastic energy E_{me} comes from the strain dependence of the magnetocrystalline anisotropy energy (MAE) E_K [34, 35]. Performing a Taylor expansion of E_K in the strain we have

$$
E_K = E_K^0 + \sum_{i=1}^{6} \left(\frac{\partial E_K}{\partial \tilde{\varepsilon}_i} \right)_0 \tilde{\varepsilon}_i + \frac{1}{2} \sum_{i,j=1}^{6} \left(\frac{\partial^2 E_K}{\partial \tilde{\varepsilon}_i \partial \tilde{\varepsilon}_j} \right)_0 \tilde{\varepsilon}_i \tilde{\varepsilon}_j + O(\tilde{\varepsilon}^3), \tag{10}
$$

where E_K^0 corresponds to the MAE of the undeformed state that contains the magnetocrystalline anisotropy constants K. The third term in the right hand side of Eq.10 is the second-order magnetoelastic energy that leads to a very small additional contribution to the second-order elastic energy given by Eq.9, so that is usually neglected [34, 36]. The first-order magnetoelastic energy

$$
E_{me} = \sum_{i=1}^{6} \left(\frac{\partial E_K}{\partial \tilde{\varepsilon}_i} \right)_0 \tilde{\varepsilon}_i \tag{11}
$$

is obtained by taking the direct product of the symmetry strains and direction cosine polynomial for each irreducible representation, multiplying by a constant, called the magnetoelastic constant and finally summing over the different representations [5, 8, 16, 17]. Frequently, the first-order magnetoelastic energy is considered up to second-order of the direction cosine polynomial α. In cartesian coordinates, it may be written as

$$
E_{me} = \sum_{i=1}^{3} g_i(\alpha^0) \tilde{\varepsilon}_i + \sum_{i=1}^{6} f_i(\alpha^2) \tilde{\varepsilon}_i + O(\alpha^4), \tag{12}
$$

6

Table 1: Number of independent second-order elastic constants of each crystal system. Number of independent magnetoelastic and magnetostrictive coefficients up to second-order of the direction cosine polynomial in the first-order magnetoelastic energy. In the last column we specify which crystal systems are supported by the current version of MAELAS.

Crystal system	Point groups	Space groups	Elastic constants (C_{ij})	Magnetoelastic constants (b)	Magnetostriction coefficients (λ)	MAELAS
Triclinic	$1, \bar{1}$	$1 - 2$	21	36	36	No
Monoclinic	$2, m, 2/m$	$3 - 15$	13	20	20	No
Orthorhombic	$222, 2mm, mmm$	$16 - 74$	9	12	12	Yes
Tetragonal (II)	$4, \bar{4}, 4/m$	$75 - 88$	7	10	10	No
Tetragonal (I)	$4mm, 422, \bar{4}2m, 4/mmm$	$89 - 142$	6	7	7	Yes
Trigonal (II)	$3, \bar{3}$	$143 - 148$	7	12	12	No
Trigonal (I)	$32, 3m, \bar{3}m$	$149 - 167$	6	8	8	Yes
Hexagonal(II)	$6, \bar{6}, 6/m$	$168 - 176$	5	8	8	No
Hexagonal (I)	$6mm, 622, \bar{6}2m, 6/mmm$	$177 - 194$	5	6	6	Yes
Cubic (II)	$23, m\bar{3}$	$195 - 206$	3	4	4	No
Cubic (I)	$432, \bar{4}3m, m\bar{3}m$	$207 - 230$	3	3	3	Yes

where functions g_i and f_i contain the magnetoelastic constants (b). In the following subsections, we show the form of Eqs.1, 9 and 12 for the main crystal symmetries studied in magnetostriction, which are implemented in the program MAELAS. The remaining crystal systems not discussed here might be included in the new versions of the code. In Table 1, we present a summary of the crystal systems supported by MAELAS. Here, we use the notation of Wallace [37, 38] (I/II) to distinguish Laue classes within the same crystal system.

Before analyzing each crystal system, we must make an important remark about the notation for the strain tensor ε_{ij}. In previous works discussing magnetostriction like Refs.[5, 8, 35], the Voigt definition of the strain tensor was used ($\varepsilon_{ij}^V, i, j = x, y, z$) [39], which is related to the one defined in the present work as $\varepsilon_{ii} = \varepsilon_{ii}^V$, $2\varepsilon_{ij} = \varepsilon_{ij}^V, i \neq j$. Consequently, the following elastic and magnetoelastic energies (in terms of the strain tensor with two cartesian indices) contain numerical factors different to those given in Kittel and Clark works [5, 35] for the terms with non-diagonal elements of the strain tensor ($\varepsilon_{ij}, i \neq j$). The following expressions for the relative length change ($\Delta l/l_0$) are the same as in Kittel and Clark works [5, 35] because the sum in Eq.1 runs over all possible values of indices $i, j = x, y, z$, while in Kittel and Clark works [5, 35] the sum runs up to $i \geqslant j$. In the present work, the equations of magnetostrictive coefficients expressed in terms of the elastic and magnetoelastic constants are also the same to those given in Kittel and Clark works [5, 35].

2.1. Cubic (I)

2.1.1. Single crystal

For cubic (I) systems (point groups 432, $\bar{4}3m$, $m\bar{3}m$) the elastic stiffness tensor reads

$$C^{cub} = \begin{pmatrix} C_{11} & C_{12} & C_{12} & 0 & 0 & 0 \\ C_{12} & C_{11} & C_{12} & 0 & 0 & 0 \\ C_{12} & C_{12} & C_{11} & 0 & 0 & 0 \\ 0 & 0 & 0 & C_{44} & 0 & 0 \\ 0 & 0 & 0 & 0 & C_{44} & 0 \\ 0 & 0 & 0 & 0 & 0 & C_{44} \end{pmatrix}, \tag{13}$$

so there are three independent elastic constants C_{11}, C_{12} and C_{44}. Hence, the elastic energy Eq.9 becomes

$$\begin{aligned} \frac{E_{el}^{cub} - E_0}{V_0} &= \frac{C_{11}}{2}(\tilde{\varepsilon}_1^2 + \tilde{\varepsilon}_2^2 + \tilde{\varepsilon}_3^2) + C_{12}(\tilde{\varepsilon}_1\tilde{\varepsilon}_2 + \tilde{\varepsilon}_1\tilde{\varepsilon}_3 + \tilde{\varepsilon}_2\tilde{\varepsilon}_3) \\ &\quad + \frac{C_{44}}{2}(\tilde{\varepsilon}_4^2 + \tilde{\varepsilon}_5^2 + \tilde{\varepsilon}_6^2) \\ &= \frac{c_{xxxx}}{2}(\varepsilon_{xx}^2 + \varepsilon_{yy}^2 + \varepsilon_{zz}^2) + c_{xxyy}(\varepsilon_{xx}\varepsilon_{yy} + \varepsilon_{xx}\varepsilon_{zz} + \varepsilon_{yy}\varepsilon_{zz}) \\ &\quad + 2c_{yzyz}(\varepsilon_{xy}^2 + \varepsilon_{yz}^2 + \varepsilon_{xz}^2), \end{aligned} \tag{14}$$

where $C_{11} = c_{xxxx}$, $C_{12} = c_{xxyy}$ and $C_{44} = c_{yzyz}$. On the other hand, the first-order magnetoelastic energy up to second-order direction cosine polynomial contains 3 magnetoelastic constants [17]. From the symmetry strains and direction cosine polynomial for each irreducible representation, it is possible to obtain the following magnetoelastic energy in cartesian coordinates [5, 8, 10]

$$\begin{aligned} \frac{E_{me}^{cub(I)}}{V_0} &= b_0(\tilde{\varepsilon}_1 + \tilde{\varepsilon}_2 + \tilde{\varepsilon}_3) + b_1(\alpha_x^2\tilde{\varepsilon}_1 + \alpha_y^2\tilde{\varepsilon}_2 + \alpha_z^2\tilde{\varepsilon}_3) \\ &\quad + b_2(\alpha_x\alpha_y\tilde{\varepsilon}_6 + \alpha_x\alpha_z\tilde{\varepsilon}_5 + \alpha_y\alpha_z\tilde{\varepsilon}_4) \\ &= b_0(\varepsilon_{xx} + \varepsilon_{yy} + \varepsilon_{zz}) + b_1(\alpha_x^2\varepsilon_{xx} + \alpha_y^2\varepsilon_{yy} + \alpha_z^2\varepsilon_{zz}) \\ &\quad + 2b_2(\alpha_x\alpha_y\varepsilon_{xy} + \alpha_x\alpha_z\varepsilon_{xz} + \alpha_y\alpha_z\varepsilon_{yz}), \end{aligned} \tag{15}$$

where b_0 is the volume magnetoelastic constant, and b_1 and b_2 are the anisotropic magnetoelastic constants. Next, replacing Eqs.14 and 15 into Eq.3, we find the

following equilibrium strains

$$\varepsilon_{ij}^{eq} = -\frac{b_2 \alpha_i \alpha_j}{2C_{44}}, \qquad i \neq j, \qquad i,j = x,y,z$$

$$\varepsilon_{ii}^{eq} = -\frac{b_1 \alpha_i^2}{C_{11} - C_{12}} - \frac{b_0}{C_{11} + 2C_{12}} + \frac{b_1 C_{12}}{(C_{11} - C_{12})(C_{11} + 2C_{12})}, \qquad i = x,y,z$$

(16)

Inserting these equilibrium strains into Eq.1 gives

$$\left. \frac{\Delta l}{l_0} \right|_{\boldsymbol{\beta}}^{\boldsymbol{\alpha}} = \lambda^{\alpha} + \frac{3}{2}\lambda_{001}\left(\alpha_x^2 \beta_x^2 + \alpha_y^2 \beta_y^2 + \alpha_z^2 \beta_z^2 - \frac{1}{3}\right)$$
$$+ 3\lambda_{111}(\alpha_x \alpha_y \beta_x \beta_y + \alpha_y \alpha_z \beta_y \beta_z + \alpha_x \alpha_z \beta_x \beta_z),$$

(17)

where

$$\lambda^{\alpha} = \frac{-b_0 - \frac{1}{3}b_1}{C_{11} + 2C_{12}},$$
$$\lambda_{001} = \frac{-2b_1}{3(C_{11} - C_{12})},$$
$$\lambda_{111} = \frac{-b_2}{3C_{44}}.$$

(18)

The coefficient λ^{α} describes the volume magnetostriction, while λ_{001} and λ_{111} are the anisotropic magnetostrictive coefficients that give the fractional length change along the [001] and [111] directions when a demagnetized material is magnetized in these directions, respectively. The superscript α in λ^{α} stands for one irreducible representation of the group of transformations which take the crystal into itself [5, 8], so it should not be confused with the direction of magnetization $\boldsymbol{\alpha}$. The MAE in an unstrained cubic crystal up to sixth-order of direction cosine polynomial is [35, 40]

$$\frac{E_K^0}{V_0} = K_0 + K_1(\alpha_x^2 \alpha_y^2 + \alpha_x^2 \alpha_z^2 + \alpha_y^2 \alpha_z^2) + K_2 \alpha_x^2 \alpha_y^2 \alpha_z^2,$$

(19)

where K_0, K_1 and K_2 are the magnetocrystalline anisotropy constants.

2.1.2. Polycrystal

The theory of magnetostriction for polycrystalline materials is more complex than for single crystals. A widely used approximation is to assume that the stress distribution is uniform through the material. In this case the relative change in

9

length may be put into the form [8, 13, 34, 41]

$$\frac{\Delta l}{l_0}\bigg|_{\boldsymbol{\beta}}^{\boldsymbol{\alpha}} = \frac{3}{2}\lambda_S\left[(\boldsymbol{\alpha}\cdot\boldsymbol{\beta})^2 - \frac{1}{3}\right],\tag{20}$$

where

$$\lambda_S = \frac{2}{5}\lambda_{001} + \frac{3}{5}\lambda_{111}.\tag{21}$$

This result is analogous to the Reuss approximation used in the elastic theory of polycrystals to obtain a lower bound of bulk and shear modulus [8, 42–44]. A discussion about the limitations of this approximation can be found in Ref.[45].

2.2. Hexagonal (I)

2.2.1. Single crystal

The elastic stiffness tensor for hexagonal (I) system (point groups 6mm, 622, $\bar{6}2m$, 6/mmm) reads

$$C^{hex} = \begin{pmatrix} C_{11} & C_{12} & C_{13} & 0 & 0 & 0 \\ C_{12} & C_{11} & C_{13} & 0 & 0 & 0 \\ C_{13} & C_{13} & C_{33} & 0 & 0 & 0 \\ 0 & 0 & 0 & C_{44} & 0 & 0 \\ 0 & 0 & 0 & 0 & C_{44} & 0 \\ 0 & 0 & 0 & 0 & 0 & \frac{C_{11}-C_{12}}{2} \end{pmatrix},\tag{22}$$

so that it has five independent elastic constants C_{11}, C_{12}, C_{13}, C_{33} and C_{44}. As a result, the elastic energy Eq.9 is

$$\begin{aligned}\frac{E_{el}^{hex} - E_0}{V_0} &= \frac{1}{2}C_{11}(\tilde{\varepsilon}_1^2 + \tilde{\varepsilon}_2^2) + C_{12}\tilde{\varepsilon}_1\tilde{\varepsilon}_2 + C_{13}(\tilde{\varepsilon}_1 + \tilde{\varepsilon}_2)\tilde{\varepsilon}_3 + \frac{1}{2}C_{33}\tilde{\varepsilon}_3^2 \\ &\quad + \frac{1}{2}C_{44}(\tilde{\varepsilon}_4^2 + \tilde{\varepsilon}_5^2) + \frac{1}{4}(C_{11} - C_{12})\tilde{\varepsilon}_6^2 \\ &= \frac{1}{2}c_{xxxx}(\varepsilon_{xx}^2 + \varepsilon_{yy}^2) + c_{xxyy}\varepsilon_{xx}\varepsilon_{yy} + c_{xxzz}(\varepsilon_{xx} + \varepsilon_{yy})\varepsilon_{zz} + \frac{1}{2}c_{zzzz}\varepsilon_{zz}^2 \\ &\quad + 2c_{yzyz}(\varepsilon_{yz}^2 + \varepsilon_{xz}^2) + (c_{xxxx} - c_{xxyy})\varepsilon_{xy}^2\end{aligned}\tag{23}$$

where $C_{11} = c_{xxxx}$, $C_{12} = c_{xxyy}$, $C_{13} = c_{xxzz}$, $C_{33} = c_{zzzz}$, and $C_{44} = c_{yzyz}$. The first order magnetoelastic energy up to quadratic direction cosine polynomial contains

10

6 magnetoelastic constants [17]. In cartesian coordinates it can be written as [5]

$$
\frac{E_{me}^{hex(I)}}{V_0} = b_{11}(\varepsilon_{xx}+\varepsilon_{yy}) + b_{12}\varepsilon_{zz} + b_{21}\left(\alpha_z^2 - \frac{1}{3}\right)(\varepsilon_{xx}+\varepsilon_{yy}) + b_{22}\left(\alpha_z^2 - \frac{1}{3}\right)\varepsilon_{zz}
$$
$$
+ b_3\left[\frac{1}{2}(\alpha_x^2 - \alpha_y^2)(\varepsilon_{xx}-\varepsilon_{yy}) + 2\alpha_x\alpha_y\varepsilon_{xy}\right] + 2b_4(\alpha_x\alpha_z\varepsilon_{xz} + \alpha_y\alpha_z\varepsilon_{yz}).
$$

(24)

Once the equilibrium strains are calculated by minimizing Eqs.23 and 24 through Eq.3 and inserted into Eq.1, one finds [5, 8, 16]

$$
\left.\frac{\Delta l}{l_0}\right|_\beta^\alpha = \lambda^{\alpha 1,0}(\beta_x^2 + \beta_y^2) + \lambda^{\alpha 2,0}\beta_z^2 + \lambda^{\alpha 1,2}\left(\alpha_z^2 - \frac{1}{3}\right)(\beta_x^2 + \beta_y^2)
$$
$$
+ \lambda^{\alpha 2,2}\left(\alpha_z^2 - \frac{1}{3}\right)\beta_z^2 + \lambda^{\gamma,2}\left[\frac{1}{2}(\alpha_x^2 - \alpha_y^2)(\beta_x^2 - \beta_y^2) + 2\alpha_x\alpha_y\beta_x\beta_y\right]
$$
$$
+ 2\lambda^{\varepsilon,2}(\alpha_x\alpha_z\beta_x\beta_z + \alpha_y\alpha_z\beta_y\beta_z),
$$

(25)

where

$$
\lambda^{\alpha 1,0} = \frac{b_{11}C_{33} + b_{12}C_{13}}{C_{33}(C_{11}+C_{12}) - 2C_{13}^2},
$$
$$
\lambda^{\alpha 2,0} = \frac{2b_{11}C_{13} - b_{12}(C_{11}+C_{12})}{C_{33}(C_{11}+C_{12}) - 2C_{13}^2},
$$
$$
\lambda^{\alpha 1,2} = \frac{-b_{21}C_{33} + b_{22}C_{13}}{C_{33}(C_{11}+C_{12}) - 2C_{13}^2},
$$
$$
\lambda^{\alpha 2,2} = \frac{2b_{21}C_{13} - b_{22}(C_{11}+C_{12})}{C_{33}(C_{11}+C_{12}) - 2C_{13}^2},
$$
$$
\lambda^{\gamma,2} = \frac{-b_3}{C_{11} - C_{12}},
$$
$$
\lambda^{\varepsilon,2} = \frac{-b_4}{2C_{44}}.
$$

(26)

These magnetostrictive coefficients are related to the normal strain modes for a cylinder [5, 8]. The equation of the relative length change in the form of Eq.25 was proposed by Clark et al. [16]. In literature there are different arrangements of the right hand side of Eq.25 that leads to other definitions of the magnetostrictive coefficients, like those defined by Mason [15], Birss [34], and Callen and Callen [17]. The conversion formulas between Eq.25 and all these other conventions can

be found in Appendix A. These conversion formulas are implemented in the program MAELAS, so that the magnetostrictive coefficients are also given according to these definitions. Note that in some works [40, 45] the magnetostrictive coefficients $\lambda^{\gamma,2}$ and $\lambda^{\varepsilon,2}$ in Eq.25 are named as $\lambda^{\varepsilon,2}$ and $\lambda^{\zeta,2}$, respectively, which is more consistent with the Bethe's group-theoretical notation [45]. The MAE in an unstrained hexagonal crystal up to fourth-order of α reads [40]

$$\frac{E_K^0}{V_0} = K_0 + K_1(1-\alpha_z^2) + K_2(1-\alpha_z^2)^2. \tag{27}$$

2.2.2. Polycrystal

Under the assumption of uniform stress, the relative change in length for polycrystalline hexagonal (I) systems can be written as [34]

$$\left.\frac{\Delta l}{l_0}\right|_{\boldsymbol{\beta}}^{\boldsymbol{\alpha}} = \xi + \eta(\boldsymbol{\alpha}\cdot\boldsymbol{\beta})^2, \tag{28}$$

where η is, in both easy axis and easy plane MAE, given by

$$\eta = -\frac{2}{15}Q_4 + \frac{1}{5}Q_6 + \frac{7}{15}Q_8. \tag{29}$$

The quantity ξ is different for easy axis and easy plane. In the case of easy axis, ξ is given by

$$\xi = \frac{2}{3}Q_2 + \frac{4}{15}Q_4 - \frac{1}{15}Q_6 + \frac{1}{15}Q_8, \qquad \text{(easy axis)} \tag{30}$$

while for easy plane is

$$\xi = -\frac{1}{3}Q_2 - \frac{1}{15}Q_4 - \frac{1}{15}Q_6 - \frac{4}{15}Q_8. \qquad \text{(easy plane)} \tag{31}$$

The quantities Q_i ($i = 2, 4, 6, 8$) are the anisotropic magnetostrictive coefficients in Birss's convention [34], and are related to the magnetostrictive coefficients defined in Eq. 25 through Eq. A.4. We have implemented these formulas in MAELAS, so that it also calculates η and ξ.

2.3. Trigonal (I)

2.3.1. Single crystal

The elastic stiffness tensor for trigonal (I) system (point groups 32, 3*m*, $\bar{3}m$) has 6 independent elastic constants C_{11}, C_{12}, C_{13}, C_{33}, C_{44} and C_{14}, and it is given

by

$$C^{trig(I)} = \begin{pmatrix} C_{11} & C_{12} & C_{13} & C_{14} & 0 & 0 \\ C_{12} & C_{11} & C_{13} & -C_{14} & 0 & 0 \\ C_{13} & C_{13} & C_{33} & 0 & 0 & 0 \\ C_{14} & -C_{14} & 0 & C_{44} & 0 & 0 \\ 0 & 0 & 0 & 0 & C_{44} & C_{14} \\ 0 & 0 & 0 & 0 & C_{14} & \frac{C_{11}-C_{12}}{2} \end{pmatrix}. \tag{32}$$

Hence, inserting this tensor into Eq.9 we have the following elastic energy

$$
\begin{aligned}
\frac{E_{el}^{trig(I)} - E_0}{V_0} &= \frac{1}{2}C_{11}(\tilde{\varepsilon}_1^2 + \tilde{\varepsilon}_2^2) + C_{12}\tilde{\varepsilon}_1\tilde{\varepsilon}_2 + C_{13}(\tilde{\varepsilon}_1 + \tilde{\varepsilon}_2)\tilde{\varepsilon}_3 + \frac{1}{2}C_{33}\tilde{\varepsilon}_3^2 \\
&\quad + \frac{1}{2}C_{44}(\tilde{\varepsilon}_5^2 + \tilde{\varepsilon}_4^2) + \frac{1}{4}(C_{11} - C_{12})\tilde{\varepsilon}_6^2 + C_{14}(\tilde{\varepsilon}_6\tilde{\varepsilon}_5 + \tilde{\varepsilon}_1\tilde{\varepsilon}_4 - \tilde{\varepsilon}_2\tilde{\varepsilon}_4). \\
&= \frac{1}{2}c_{xxxx}(\varepsilon_{xx}^2 + \varepsilon_{yy}^2) + c_{xxyy}\varepsilon_{xx}\varepsilon_{yy} + c_{xxzz}(\varepsilon_{xx} + \varepsilon_{yy})\varepsilon_{zz} + \frac{1}{2}c_{zzzz}\varepsilon_{zz}^2 \\
&\quad + 2c_{yzyz}(\varepsilon_{xz}^2 + \varepsilon_{yz}^2) + (c_{xxxx} - c_{xxyy})\varepsilon_{xy}^2 + 4c_{xxyz}(\varepsilon_{xy}\varepsilon_{xz} + \varepsilon_{xx}\varepsilon_{yz} - \varepsilon_{yy}\varepsilon_{yz}).
\end{aligned}
\tag{33}
$$

where $C_{11} = c_{xxxx}$, $C_{12} = c_{xxyy}$, $C_{13} = c_{xxzz}$, $C_{14} = c_{xxyz}$, $C_{33} = c_{zzzz}$, and $C_{44} = c_{yzyz}$. On the other hand, the magnetoelastic energy contains 8 independent magnetoelastic constants [17]. In cartesian coordinates it can be written as [8]

$$
\begin{aligned}
\frac{E_{me}^{trig(I)}}{V_0} &= b_{11}(\varepsilon_{xx} + \varepsilon_{yy}) + b_{12}\varepsilon_{zz} + b_{21}\left(\alpha_z^2 - \frac{1}{3}\right)(\varepsilon_{xx} + \varepsilon_{yy}) + b_{22}\left(\alpha_z^2 - \frac{1}{3}\right)\varepsilon_{zz} \\
&\quad + b_3\left[\frac{1}{2}(\alpha_x^2 - \alpha_y^2)(\varepsilon_{xx} - \varepsilon_{yy}) + 2\alpha_x\alpha_y\varepsilon_{xy}\right] + 2b_4(\alpha_x\alpha_z\varepsilon_{xz} + \alpha_y\alpha_z\varepsilon_{yz}) \\
&\quad + b_{14}\left[(\alpha_x^2 - \alpha_y^2)\varepsilon_{yz} + 2\alpha_x\alpha_y\varepsilon_{xz}\right] + b_{34}\left[\frac{1}{2}\alpha_y\alpha_z(\varepsilon_{xx} - \varepsilon_{yy}) + 2\alpha_x\alpha_z\varepsilon_{xy}\right].
\end{aligned}
\tag{34}
$$

Next, we obtain the equilibrium strains via Eq.3. Replacing them into Eq.1 leads to [8]

$$
\begin{aligned}
\left.\frac{\Delta l}{l_0}\right|_{\beta}^{\alpha} &= \lambda^{\alpha 1,0}(\beta_x^2 + \beta_y^2) + \lambda^{\alpha 2,0}\beta_z^2 + \lambda^{\alpha 1,2}\left(\alpha_z^2 - \frac{1}{3}\right)(\beta_x^2 + \beta_y^2) \\
&+ \lambda^{\alpha 2,2}\left(\alpha_z^2 - \frac{1}{3}\right)\beta_z^2 + \lambda^{\gamma,1}\left[\frac{1}{2}(\alpha_x^2 - \alpha_y^2)(\beta_x^2 - \beta_y^2) + 2\alpha_x\alpha_y\beta_x\beta_y\right] \\
&+ \lambda^{\gamma,2}(\alpha_x\alpha_z\beta_x\beta_z + \alpha_y\alpha_z\beta_y\beta_z) + \lambda_{12}\left[\frac{1}{2}\alpha_y\alpha_z(\beta_x^2 - \beta_y^2) + \alpha_x\alpha_z\beta_x\beta_y\right] \\
&+ \lambda_{21}\left[\frac{1}{2}(\alpha_x^2 - \alpha_y^2)\beta_y\beta_z + \alpha_x\alpha_y\beta_x\beta_z\right],
\end{aligned}
\tag{35}
$$

where

$$
\begin{aligned}
\lambda^{\alpha 1,0} &= \frac{b_{11}C_{33} + b_{12}C_{13}}{C_{33}(C_{11} + C_{12}) - 2C_{13}^2}, \\
\lambda^{\alpha 2,0} &= \frac{2b_{11}C_{13} - b_{12}(C_{11} + C_{12})}{C_{33}(C_{11} + C_{12}) - 2C_{13}^2}, \\
\lambda^{\alpha 1,2} &= \frac{-b_{21}C_{33} + b_{22}C_{13}}{C_{33}(C_{11} + C_{12}) - 2C_{13}^2}, \\
\lambda^{\alpha 2,2} &= \frac{2b_{21}C_{13} - b_{22}(C_{11} + C_{12})}{C_{33}(C_{11} + C_{12}) - 2C_{13}^2}, \\
\lambda^{\gamma,1} &= \frac{C_{14}b_{14} - C_{44}b_3}{\frac{1}{2}C_{44}(C_{11} - C_{12}) - C_{14}^2}, \\
\lambda^{\gamma,2} &= \frac{\frac{1}{2}b_4(C_{11} - C_{12}) - b_{34}C_{14}}{\frac{1}{2}C_{44}(C_{11} - C_{12}) - C_{14}^2}, \\
\lambda_{12} &= \frac{C_{14}b_4 - C_{44}b_{34}}{\frac{1}{2}C_{44}(C_{11} - C_{12}) - C_{14}^2}, \\
\lambda_{21} &= \frac{\frac{1}{2}b_{14}(C_{11} - C_{12}) - b_3C_{14}}{\frac{1}{2}C_{44}(C_{11} - C_{12}) - C_{14}^2}.
\end{aligned}
\tag{36}
$$

The MAE in an unstrained trigonal crystal up to fourth-order in α is the same to the hexagonal case (Eq.27).

2.4. Tetragonal (I)

2.4.1. Single crystal

The tetragonal (I) crystal system (point groups $4mm$, 422, $\bar{4}2m$, $4/mmm$) has the following elastic stiffness tensor

$$
C^{tet(I)} = \begin{pmatrix}
C_{11} & C_{12} & C_{13} & 0 & 0 & 0 \\
C_{12} & C_{11} & C_{13} & 0 & 0 & 0 \\
C_{13} & C_{13} & C_{33} & 0 & 0 & 0 \\
0 & 0 & 0 & C_{44} & 0 & 0 \\
0 & 0 & 0 & 0 & C_{44} & 0 \\
0 & 0 & 0 & 0 & 0 & C_{66}
\end{pmatrix},
\tag{37}
$$

Hence, it has six independent elastic constants C_{11}, C_{12}, C_{13}, C_{33}, C_{44} and C_{66}. The elastic energy is given by

$$
\begin{aligned}
\frac{E_{el}^{tet(I)} - E_0}{V_0} &= \frac{1}{2}C_{11}(\tilde{\varepsilon}_1^2 + \tilde{\varepsilon}_2^2) + C_{12}\tilde{\varepsilon}_1\tilde{\varepsilon}_2 + C_{13}(\tilde{\varepsilon}_1 + \tilde{\varepsilon}_2)\tilde{\varepsilon}_3 + \frac{1}{2}C_{33}\tilde{\varepsilon}_3^2 \\
&\quad + \frac{1}{2}C_{44}(\tilde{\varepsilon}_4^2 + \tilde{\varepsilon}_5^2) + \frac{1}{2}C_{66}\tilde{\varepsilon}_6^2 \\
&= \frac{1}{2}c_{xxxx}(\varepsilon_{xx}^2 + \varepsilon_{yy}^2) + c_{xxyy}\varepsilon_{xx}\varepsilon_{yy} + c_{xxzz}(\varepsilon_{xx} + \varepsilon_{yy})\varepsilon_{zz} + \frac{1}{2}c_{zzzz}\varepsilon_{zz}^2 \\
&\quad + 2c_{yzyz}(\varepsilon_{yz}^2 + \varepsilon_{xz}^2) + 2c_{xyxy}\varepsilon_{xy}^2
\end{aligned}
\tag{38}
$$

where $C_{11} = c_{xxxx}$, $C_{12} = c_{xxyy}$, $C_{13} = c_{xxzz}$, $C_{33} = c_{zzzz}$, $C_{44} = c_{yzyz}$ and $C_{66} = c_{xyxy}$. On the other hand, there are 7 independent magnetoelastic constants [17]. The magnetoelastic energy can be written as [8, 10]

$$
\begin{aligned}
\frac{E_{me}^{tet(I)}}{V_0} &= b_{11}(\varepsilon_{xx} + \varepsilon_{yy}) + b_{12}\varepsilon_{zz} + b_{21}\left(\alpha_z^2 - \frac{1}{3}\right)(\varepsilon_{xx} + \varepsilon_{yy}) + b_{22}\left(\alpha_z^2 - \frac{1}{3}\right)\varepsilon_{zz} \\
&\quad + \frac{1}{2}b_3(\alpha_x^2 - \alpha_y^2)(\varepsilon_{xx} - \varepsilon_{yy}) + 2b_3'\alpha_x\alpha_y\varepsilon_{xy} + 2b_4(\alpha_x\alpha_z\varepsilon_{xz} + \alpha_y\alpha_z\varepsilon_{yz}).
\end{aligned}
\tag{39}
$$

15

After the equilibrium strains are calculated by minimizing Eqs.38 and 39 through Eq.3 and replaced into Eq.1, we have [8]

$$
\left.\frac{\Delta l}{l_0}\right|_{\boldsymbol{\beta}}^{\boldsymbol{\alpha}} = \lambda^{\alpha 1,0}(\beta_x^2 + \beta_y^2) + \lambda^{\alpha 2,0}\beta_z^2 + \lambda^{\alpha 1,2}\left(\alpha_z^2 - \frac{1}{3}\right)(\beta_x^2 + \beta_y^2)
$$

$$
+ \lambda^{\alpha 2,2}\left(\alpha_z^2 - \frac{1}{3}\right)\beta_z^2 + \frac{1}{2}\lambda^{\gamma,2}(\alpha_x^2 - \alpha_y^2)(\beta_x^2 - \beta_y^2) + 2\lambda^{\delta,2}\alpha_x\alpha_y\beta_x\beta_y
$$

$$
+ 2\lambda^{\varepsilon,2}(\alpha_x\alpha_z\beta_x\beta_z + \alpha_y\alpha_z\beta_y\beta_z),
$$

(40)

where

$$
\lambda^{\alpha 1,0} = \frac{b_{11}C_{33} + b_{12}C_{13}}{C_{33}(C_{11} + C_{12}) - 2C_{13}^2},
$$

$$
\lambda^{\alpha 2,0} = \frac{2b_{11}C_{13} - b_{12}(C_{11} + C_{12})}{C_{33}(C_{11} + C_{12}) - 2C_{13}^2},
$$

$$
\lambda^{\alpha 1,2} = \frac{-b_{21}C_{33} + b_{22}C_{13}}{C_{33}(C_{11} + C_{12}) - 2C_{13}^2},
$$

$$
\lambda^{\alpha 2,2} = \frac{2b_{21}C_{13} - b_{22}(C_{11} + C_{12})}{C_{33}(C_{11} + C_{12}) - 2C_{13}^2},
$$

(41)

$$
\lambda^{\gamma,2} = \frac{-b_3}{C_{11} - C_{12}},
$$

$$
\lambda^{\delta,2} = \frac{-b_3'}{2C_{66}},
$$

$$
\lambda^{\varepsilon,2} = \frac{-b_4}{2C_{44}}.
$$

Mason derived an equivalent equation to Eq.40 using a different arrangement of the terms and definitions of the magnetostrictive coefficients [15]. The conversion formulas between the magnetostrictive coefficients in Eq.40 and those defined by Mason are shown in Appendix B. The MAE in an unstrained tetragonal crystal up to fourth-order in α is the same to the hexagonal case (Eq.27).

2.5. Orthorhombic

2.5.1. Single crystal

The orthorhombic crystal system (point groups 222, *2mm*, *mmm*) has 9 independent elastic constants C_{11}, C_{12}, C_{13}, C_{22}, C_{23}, C_{33}, C_{44}, C_{55} and C_{66}, its elastic

stiffness matrix reads[38, 44]

$$C^{ortho} = \begin{pmatrix} C_{11} & C_{12} & C_{13} & 0 & 0 & 0 \\ C_{12} & C_{22} & C_{23} & 0 & 0 & 0 \\ C_{13} & C_{23} & C_{33} & 0 & 0 & 0 \\ 0 & 0 & 0 & C_{44} & 0 & 0 \\ 0 & 0 & 0 & 0 & C_{55} & 0 \\ 0 & 0 & 0 & 0 & 0 & C_{66} \end{pmatrix}, \tag{42}$$

Hence, inserting it into Eq.9 leads to the following expression for the elastic energy

$$
\begin{aligned}
\frac{E_{el}^{ortho} - E_0}{V_0} &= \frac{1}{2}C_{11}\tilde{\varepsilon}_1^2 + \frac{1}{2}C_{22}\tilde{\varepsilon}_2^2 + C_{12}\tilde{\varepsilon}_1\tilde{\varepsilon}_2 + C_{13}\tilde{\varepsilon}_1\tilde{\varepsilon}_3 + C_{23}\tilde{\varepsilon}_2\tilde{\varepsilon}_3 + \frac{1}{2}C_{33}\tilde{\varepsilon}_3^2 \\
&\quad + \frac{1}{2}C_{44}\tilde{\varepsilon}_4^2 + \frac{1}{2}C_{55}\tilde{\varepsilon}_5^2 + \frac{1}{2}C_{66}\tilde{\varepsilon}_6^2 \\
&= \frac{1}{2}c_{xxxx}\varepsilon_{xx}^2 + \frac{1}{2}c_{yyyy}\varepsilon_{yy}^2 + c_{xxyy}\varepsilon_{xx}\varepsilon_{yy} + c_{xxzz}\varepsilon_{xx}\varepsilon_{zz} + c_{yyzz}\varepsilon_{yy}\varepsilon_{zz} \\
&\quad + \frac{1}{2}c_{zzzz}\varepsilon_{zz}^2 + 2c_{yzyz}\varepsilon_{yz}^2 + 2c_{xzxz}\varepsilon_{xz}^2 + 2c_{xyxy}\varepsilon_{xy}^2.
\end{aligned}
\tag{43}
$$

where $C_{11} = c_{xxxx}$, $C_{22} = c_{yyyy}$, $C_{12} = c_{xxyy}$, $C_{13} = c_{xxzz}$, $C_{23} = c_{yyzz}$, $C_{33} = c_{zzzz}$, $C_{44} = c_{yzyz}$, $C_{55} = c_{xzxz}$ and $C_{66} = c_{xyxy}$. The magnetoelastic energy contains 12 independent magnetoelastic constants [17]. Mason derived the following expression of the relative length change [15]

$$
\begin{aligned}
\left.\frac{\Delta l}{l_0}\right|_{\beta}^{\alpha} &= \lambda^{\alpha 1,0}\beta_x^2 + \lambda^{\alpha 2,0}\beta_y^2 + \lambda^{\alpha 3,0}\beta_z^2 + \lambda_1(\alpha_x^2\beta_x^2 - \alpha_x\alpha_y\beta_x\beta_y - \alpha_x\alpha_z\beta_x\beta_z) \\
&\quad + \lambda_2(\alpha_y^2\beta_x^2 - \alpha_x\alpha_y\beta_x\beta_y) + \lambda_3(\alpha_x^2\beta_y^2 - \alpha_x\alpha_y\beta_x\beta_y) \\
&\quad + \lambda_4(\alpha_y^2\beta_y^2 - \alpha_x\alpha_y\beta_x\beta_y - \alpha_y\alpha_z\beta_y\beta_z) + \lambda_5(\alpha_x^2\beta_z^2 - \alpha_x\alpha_z\beta_x\beta_z) \\
&\quad + \lambda_6(\alpha_y^2\beta_z^2 - \alpha_y\alpha_z\beta_y\beta_z) + 4\lambda_7\alpha_x\alpha_y\beta_x\beta_y + 4\lambda_8\alpha_x\alpha_z\beta_x\beta_z + 4\lambda_9\alpha_y\alpha_z\beta_y\beta_z.
\end{aligned}
\tag{44}
$$

Note that we added the terms that describes the volume magnetostriction ($\lambda^{\alpha 1,0}$, $\lambda^{\alpha 2,0}$ and $\lambda^{\alpha 3,0}$), which were not included in the original work of Mason [15]. The expression of the magnetoelastic energy and the relations between magnetostrictive coefficients, elastic and magnetoelastic constants were not shown by Mason either. For completeness, here we deduce it from Eqs. 43 and 44. To do so, we

aim to find the unknown functions g_i and f_i in the general form of the magnetoe-lastic energy in cartesian coordinates given by Eq. 12. Firstly, we minimize Eqs. 43 and 12 via Eq. 3. This gives a set of equations that links the unknown functions g_i and f_i with the equilibrium strains. Next, we extract the equilibrium strains by direct comparison between Eqs. 1 and 44. Finally, we substitute the equilibrium strains into the set of equations that relates g_i and f_i with the equilibrium strains, from which we obtain g_i and f_i. Inserting the calculated g_i and f_i into Eq. 12 we have

$$\frac{E_{me}^{ortho}}{V_0} = b_{01}\varepsilon_{xx} + b_{02}\varepsilon_{yy} + b_{03}\varepsilon_{zz} + b_1\alpha_x^2\varepsilon_{xx} + b_2\alpha_y^2\varepsilon_{xx} + b_3\alpha_x^2\varepsilon_{yy} + b_4\alpha_y^2\varepsilon_{yy}$$
$$+ b_5\alpha_x^2\varepsilon_{zz} + b_6\alpha_y^2\varepsilon_{zz} + 2b_7\alpha_x\alpha_y\varepsilon_{xy} + 2b_8\alpha_x\alpha_z\varepsilon_{xz} + 2b_9\alpha_y\alpha_z\varepsilon_{yz},$$

$$(45)$$

where

$$b_{01} = -C_{11}\lambda^{\alpha 1,0} - C_{12}\lambda^{\alpha 2,0} - C_{13}\lambda^{\alpha 3,0}$$
$$b_{02} = -C_{12}\lambda^{\alpha 1,0} - C_{22}\lambda^{\alpha 2,0} - C_{23}\lambda^{\alpha 3,0}$$
$$b_{03} = -C_{13}\lambda^{\alpha 1,0} - C_{23}\lambda^{\alpha 2,0} - C_{33}\lambda^{\alpha 3,0}$$
$$b_1 = -C_{11}\lambda_1 - C_{12}\lambda_3 - C_{13}\lambda_5$$
$$b_2 = -C_{11}\lambda_2 - C_{12}\lambda_4 - C_{13}\lambda_6$$
$$b_3 = -C_{12}\lambda_1 - C_{22}\lambda_3 - C_{23}\lambda_5$$
$$b_4 = -C_{12}\lambda_2 - C_{22}\lambda_4 - C_{23}\lambda_6 \qquad (46)$$
$$b_5 = -C_{13}\lambda_1 - C_{23}\lambda_3 - C_{33}\lambda_5$$
$$b_6 = -C_{13}\lambda_2 - C_{23}\lambda_4 - C_{33}\lambda_6$$
$$b_7 = C_{66}(\lambda_1 + \lambda_2 + \lambda_3 + \lambda_4 - 4\lambda_7)$$
$$b_8 = C_{55}(\lambda_1 + \lambda_5 - 4\lambda_8)$$
$$b_9 = C_{44}(\lambda_4 + \lambda_6 - 4\lambda_9).$$

Alternatively, one can deduce the magnetoelastic energy using the general approach based on the symmetry strains and direction cosine polynomial for each irreducible representation [5, 8, 17]. This approach may lead to different definitions of the magnetoelastic constants and magnetostrictive coefficients, as we have discussed for the hexagonal (I) and tetragonal (I) systems in Appendix A and Appendix B, respectively. A generalization of the approach taken by Becker and Doring [14] for orthorhombic crystals can be found in Ref. [46]. The MAE

in an unstrained orthorhombic crystal up to fourth-order in α is[15]

$$\frac{E_K^0}{V_0} = K_0 + K_1 \alpha_x^2 + K_2 \alpha_y^2. \tag{47}$$

3. Methodology

3.1. Calculation of magnetostrictive coefficients and magnetoelastic constants

The methodology implemented in the program MAELAS to calculate the anisotropic magnetostrictive coefficients is a generalization of the approach proposed by Wu and Freeman for cubic crystals [18, 19]. In this method, one measuring length direction β^i and two magnetization directions (α_1^i and α_2^i) are chosen for each magnetostrictive coefficient (λ^i) in such a way that

$$\left.\frac{\Delta l}{l_0}\right|_{\beta^i}^{\alpha_1^i} - \left.\frac{\Delta l}{l_0}\right|_{\beta^i}^{\alpha_2^i} = \rho^i \lambda^i, \tag{48}$$

where ρ^i is a real number. In Table 2 we show the selected set of β^i, α_1^i and α_2^i in MAELAS that fulfils Eq.48 for each ρ^i. Next, the left hand side of Eq.48 is written as

$$\begin{aligned}
\left.\frac{\Delta l}{l_0}\right|_{\beta^i}^{\alpha_1^i} - \left.\frac{\Delta l}{l_0}\right|_{\beta^i}^{\alpha_2^i} &= \frac{l_1 - l_0}{l_0} - \frac{l_2 - l_0}{l_0} = \frac{2(l_1 - l_2)}{(l_1 + l_2)\left[1 - \frac{l_1 + l_2 - 2l_0}{l_1 + l_2}\right]} \\
&= \frac{2(l_1 - l_2)}{l_1 + l_2}\left[1 + \frac{l_1 + l_2 - 2l_0}{l_1 + l_2} + ...\right] \approx \frac{2(l_1 - l_2)}{l_1 + l_2},
\end{aligned} \tag{49}$$

where in the last approximation we assume $|l_{1(2)} - l_0|/l_0 \ll 1$. This assumption is reasonable for all known magnetostrictive materials. For instance, a very large value of $\Delta l/l_0$ is about 4.5×10^{-3} found in TbFe$_2$ (Laves phase C15) along direction [111] at $T = 0$K [6], where this approximation is fine. This approximation allows to get rid of l_0 (length along β in the macroscopic demagnetized state) which can't be calculated with DFT methods easily. Combining Eqs.48 and 49 one can write the magnetostrictive coefficients as

$$\lambda^i = \frac{2(l_1 - l_2)}{\rho^i(l_1 + l_2)}, \tag{50}$$

19

where the value of ρ^i for each λ^i is given in Table 2. The quantities l_1 and l_2 correspond to the cell length along $\boldsymbol{\beta}$ when the magnetization points to $\boldsymbol{\alpha}_1$ and $\boldsymbol{\alpha}_2$, respectively, and are calculated through an optimization of the energy. Namely, a set of deformed unit cells is firstly generated using the deformation modes described in Appendix C. For each deformed cell, the energy is calculated constraining the spins to the directions given by $\boldsymbol{\alpha}_1$ and $\boldsymbol{\alpha}_2$. Next, the energy versus the cell length along $\boldsymbol{\beta}$ for each spin direction $\boldsymbol{\alpha}_{1(2)}$ is fitted to a quadratic polynomial

$$E(\boldsymbol{\alpha}_j, l) = A_j l^2 + B_j l + C_j, \quad j = 1, 2 \tag{51}$$

where A_j, B_j and C_j ($j = 1, 2$) are fitting parameters. The minimum of this function for spin direction $\boldsymbol{\alpha}_{1(2)}$ corresponds to $l_{1(2)} = -B_{1(2)}/(2A_{1(2)})$. Once l_1 and l_2 are determined, one obtains the magnetostrictive coefficients using Eq.50. The magnetostrictive coefficients can also be written in terms of the derivative of the energy with respect l evaluated at $l = l_2$ as [20]

$$\lambda^i \approx -\frac{1}{\eta^i B_1} \cdot \frac{\partial [E(\boldsymbol{\alpha}_2, l) - E(\boldsymbol{\alpha}_1, l)]}{\partial l}\Bigg|_{l=l_2} \tag{52}$$

where B_1 is always negative. In Table 2, we see that our choice of $\boldsymbol{\beta}$ and $\boldsymbol{\alpha}_{1(2)}$ makes ρ depend on some magnetostrictive coefficients for λ_7, λ_8 and λ_9 in orthorhombic crystals. For instance, working out the coefficient λ_7 via Eq.50 we have

$$\lambda_7 = \frac{(a^2 + b^2)(l_1 - l_2)}{ab(l_1 + l_2)} - \frac{(a-b)(a[\lambda_1 + \lambda_2] - b[\lambda_3 + \lambda_4])}{4ab}, \tag{53}$$

where a and b are the relaxed (not distorted) lattice parameters of the unit cell. Here, MAELAS makes use of the values of λ_1, λ_2, λ_3 and λ_4 calculated previously in order to compute λ_7. Note that a simpler expression for λ_7 can be achieved choosing the measuring length direction $\boldsymbol{\beta} = \left(\frac{1}{\sqrt{2}}, \frac{1}{\sqrt{2}}, 0\right)$. However, from a computational point of view, it is easy to extract the cell length l along $\boldsymbol{\beta} = \left(\frac{a}{\sqrt{a^2+b^2}}, \frac{b}{\sqrt{a^2+b^2}}, 0\right)$ of each deformed cell generated with the deformation gradients discussed in Appendix C. Similarly, one can deduce the explicit equation for λ_8 and λ_9.

Lastly, if the elastic tensor is provided in the format given by the program AELAS [44], then the magnetoelastic constants (b_k) are also calculated from the relations $b_k = b_k(\lambda^i, C_{nm})$ given in Section 2.

Table 2: Selected cell length ($\boldsymbol{\beta}$) and magnetization directions ($\boldsymbol{\alpha}_1$, $\boldsymbol{\alpha}_2$) in MAELAS to calculate the anisotropic magnetostrictive coefficients according to Eq.48. The first column shows the crystal system and the corresponding lattice convention set in MAELAS based on the IEEE format [44]. The second column presents the equation of the relative length change that we used in Eq.48 for each crystal system. In the last column we show the values of the parameter ρ that is defined in Eq.48. The symbols a, b, c correspond to the lattice parameters of the relaxed (not distorted) unit cell.

Crystal system	$\frac{\Delta l}{l_0}$	Magnetostrictive coefficient	$\boldsymbol{\beta}$	$\boldsymbol{\alpha}_1$	$\boldsymbol{\alpha}_2$	ρ
Cubic (I)	Eq.17	λ_{001}	$(0,0,1)$	$(0,0,1)$	$(1,0,0)$	$\frac{3}{2}$
$\boldsymbol{a}\|\hat{\boldsymbol{x}}, \boldsymbol{b}\|\hat{\boldsymbol{y}}, \boldsymbol{c}\|\hat{\boldsymbol{z}}$		λ_{111}	$\left(\frac{1}{\sqrt{3}},\frac{1}{\sqrt{3}},\frac{1}{\sqrt{3}}\right)$	$\left(\frac{1}{\sqrt{3}},\frac{1}{\sqrt{3}},\frac{1}{\sqrt{3}}\right)$	$\left(\frac{1}{\sqrt{2}},0,\frac{-1}{\sqrt{2}}\right)$	$\frac{3}{2}$
Hexagonal (I)	Eq.25	$\lambda^{\alpha 1,2}$	$(1,0,0)$	$\left(\frac{1}{\sqrt{3}},\frac{1}{\sqrt{3}},\frac{1}{\sqrt{3}}\right)$	$\left(\frac{1}{\sqrt{2}},\frac{1}{\sqrt{2}},0\right)$	$\frac{1}{3}$
$\boldsymbol{a}\|\hat{\boldsymbol{x}}, \boldsymbol{c}\|\hat{\boldsymbol{z}}$		$\lambda^{\alpha 2,2}$	$(0,0,1)$	$(0,0,1)$	$(1,0,0)$	1
$\boldsymbol{b}=\left(-\frac{a}{2},\frac{\sqrt{3}a}{2},0\right)$		$\lambda^{\gamma,2}$	$(1,0,0)$	$(1,0,0)$	$(0,1,0)$	1
$a=b\neq c$		$\lambda^{\varepsilon,2}$	$\frac{(a,0,c)}{\sqrt{a^2+c^2}}$	$\left(\frac{1}{\sqrt{2}},0,\frac{1}{\sqrt{2}}\right)$	$\left(\frac{-1}{\sqrt{2}},0,\frac{1}{\sqrt{2}}\right)$	$\frac{2ac}{a^2+c^2}$
Trigonal (I)	Eq.35	$\lambda^{\alpha 1,2}$	$(1,0,0)$	$(0,0,1)$	$\left(\frac{1}{\sqrt{2}},\frac{1}{\sqrt{2}},0\right)$	1
$\boldsymbol{a}\|\hat{\boldsymbol{x}}, \boldsymbol{c}\|\hat{\boldsymbol{z}}$		$\lambda^{\alpha 2,2}$	$(0,0,1)$	$(0,0,1)$	$(1,0,0)$	1
$\boldsymbol{b}=\left(-\frac{a}{2},\frac{\sqrt{3}a}{2},0\right)$		$\lambda^{\gamma,1}$	$(1,0,0)$	$(1,0,0)$	$(0,1,0)$	1
$a=b\neq c$		$\lambda^{\gamma,2}$	$\frac{(a,0,c)}{\sqrt{a^2+c^2}}$	$\left(\frac{1}{\sqrt{2}},0,\frac{1}{\sqrt{2}}\right)$	$\left(\frac{1}{\sqrt{2}},0,\frac{-1}{\sqrt{2}}\right)$	$\frac{ac}{a^2+c^2}$
		λ_{12}	$\frac{(a,0,c)}{\sqrt{a^2+c^2}}$	$\left(0,\frac{1}{\sqrt{2}},\frac{1}{\sqrt{2}}\right)$	$\left(0,\frac{1}{\sqrt{2}},\frac{-1}{\sqrt{2}}\right)$	$\frac{a^2}{2(a^2+c^2)}$
		λ_{21}	$\frac{(a,0,c)}{\sqrt{a^2+c^2}}$	$\left(\frac{1}{\sqrt{2}},\frac{1}{\sqrt{2}},0\right)$	$\left(\frac{1}{\sqrt{2}},\frac{-1}{\sqrt{2}},0\right)$	$\frac{ac}{a^2+c^2}$
Tetragonal (I)	Eq.40	$\lambda^{\alpha 1,2}$	$(1,0,0)$	$\left(\frac{1}{\sqrt{3}},\frac{1}{\sqrt{3}},\frac{1}{\sqrt{3}}\right)$	$\left(\frac{1}{\sqrt{2}},\frac{1}{\sqrt{2}},0\right)$	$\frac{1}{3}$
$\boldsymbol{a}\|\hat{\boldsymbol{x}}, \boldsymbol{b}\|\hat{\boldsymbol{y}}, \boldsymbol{c}\|\hat{\boldsymbol{z}}$		$\lambda^{\alpha 2,2}$	$(0,0,1)$	$(0,0,1)$	$(1,0,0)$	1
$a=b\neq c$		$\lambda^{\gamma,2}$	$(1,0,0)$	$(1,0,0)$	$(0,1,0)$	1
		$\lambda^{\varepsilon,2}$	$\frac{(a,0,c)}{\sqrt{a^2+c^2}}$	$\left(\frac{1}{\sqrt{2}},0,\frac{1}{\sqrt{2}}\right)$	$\left(\frac{-1}{\sqrt{2}},0,\frac{1}{\sqrt{2}}\right)$	$\frac{2ac}{a^2+c^2}$
		$\lambda^{\delta,2}$	$\left(\frac{1}{\sqrt{2}},\frac{1}{\sqrt{2}},0\right)$	$\left(\frac{1}{\sqrt{2}},\frac{1}{\sqrt{2}},0\right)$	$\left(\frac{-1}{\sqrt{2}},\frac{1}{\sqrt{2}},0\right)$	1
Orthorhombic	Eq.44	λ_1	$(1,0,0)$	$(1,0,0)$	$(0,0,1)$	1
$\boldsymbol{a}\|\hat{\boldsymbol{x}}, \boldsymbol{b}\|\hat{\boldsymbol{y}}, \boldsymbol{c}\|\hat{\boldsymbol{z}}$		λ_2	$(1,0,0)$	$(0,1,0)$	$(0,0,1)$	1
$c < a < b$		λ_3	$(0,1,0)$	$(1,0,0)$	$(0,0,1)$	1
		λ_4	$(0,1,0)$	$(0,1,0)$	$(0,0,1)$	1
		λ_5	$(0,0,1)$	$(1,0,0)$	$(0,0,1)$	1
		λ_6	$(0,0,1)$	$(0,1,0)$	$(0,0,1)$	1
		λ_7	$\frac{(a,b,0)}{\sqrt{a^2+b^2}}$	$\left(\frac{1}{\sqrt{2}},\frac{1}{\sqrt{2}},0\right)$	$(0,0,1)$	$\frac{(a-b)(a[\lambda_1+\lambda_2]-b[\lambda_3+\lambda_4])+4ab\lambda_7}{2(a^2+b^2)\lambda_7}$
		λ_8	$\frac{(a,0,c)}{\sqrt{a^2+c^2}}$	$\left(\frac{1}{\sqrt{2}},0,\frac{1}{\sqrt{2}}\right)$	$(0,0,1)$	$\frac{(a-c)(a\lambda_1-c\lambda_5)+4ac\lambda_8}{2(a^2+c^2)\lambda_8}$
		λ_9	$\frac{(0,b,c)}{\sqrt{b^2+c^2}}$	$\left(0,\frac{1}{\sqrt{2}},\frac{1}{\sqrt{2}}\right)$	$(0,0,1)$	$\frac{(b-c)(b\lambda_4-c\lambda_6)+4bc\lambda_9}{2(b^2+c^2)\lambda_9}$

3.2. Program workflow

The program MAELAS has been designed to read and write files for the Vienna Ab initio Simulation Package (VASP) code [47–49]. The workflow of MAELAS can be splitted into 5 steps: (i) cell relaxation, (ii) test of MAE, (iii) generation of distorted cells and spin directions, (iv) calculation of the energy with VASP, and (v) calculation of magnetostrictive coefficients and magnetoelastic constants. In Fig.2 we show a diagram with a summary of the MAELAS workflow. In the first step, it performs a full cell relaxation (ionic positions, cell volume, and cell shape) of the input unit cell. If one wants to use non-relaxed lattice parameters (like experimental ones), then this step can be skipped. In the next step, it is recommended to check if it is possible to obtain a realistic value of MAE for the ground state (not distorted cell). To do so, MAELAS generates the VASP input files to calculate MAE for two spin directions given by the user which should be compared with available experimental data. In the third step, MAELAS performs a symmetry analysis with pymatgen library [50] to determine the crystal system, redefine the structure using the same IEEE lattice convention as in AELAS [44], and lastly generates a set of volume-conserving deformed unit cells and spin directions according to Table 2. Alternatively, the crystal symmetry of the system can also be imposed by the user manually, which could be useful in some cases. In the fourth step, one should run the VASP calculations using these inputs. In order to help in this task, MAELAS generates some bash scripts to run all calculations with VASP automatically. Lastly, MAELAS analyzes the calculated energies and fits them to a quadratic function (see Section 3.1) in order to obtain the magnetostrictive coefficients. If the elastic tensor is provided in the format given by the program AELAS [44], then the magnetoelastic constants (b_k) are also calculated from the relations $b_k = b_k(\lambda^i, C_{nm})$ given in Section 2. The obtained magnetostrictive coefficients and MAE can be further analyzed through the online visualization tool called MAELASviewer that we have also developed [51–53].

Detecting possible calculation failures on fly is a very important feature of an automated high-throughput code. For instance, MAELAS prints a warning message when the R-squared of the quadratic curve fitting is lower than 0.98. It also automatically generates figures showing the quadratic curve fitting and the energy difference between states with spin directions $\boldsymbol{\alpha}_2$ and $\boldsymbol{\alpha}_1$ versus the cell length along $\boldsymbol{\beta}$, so that the users can check the results easily.

3.3. Computational details

The MAELAS code is written in Python3, and its source and documentation files are available in GitHub repository [54]. The DFT calculations are performed
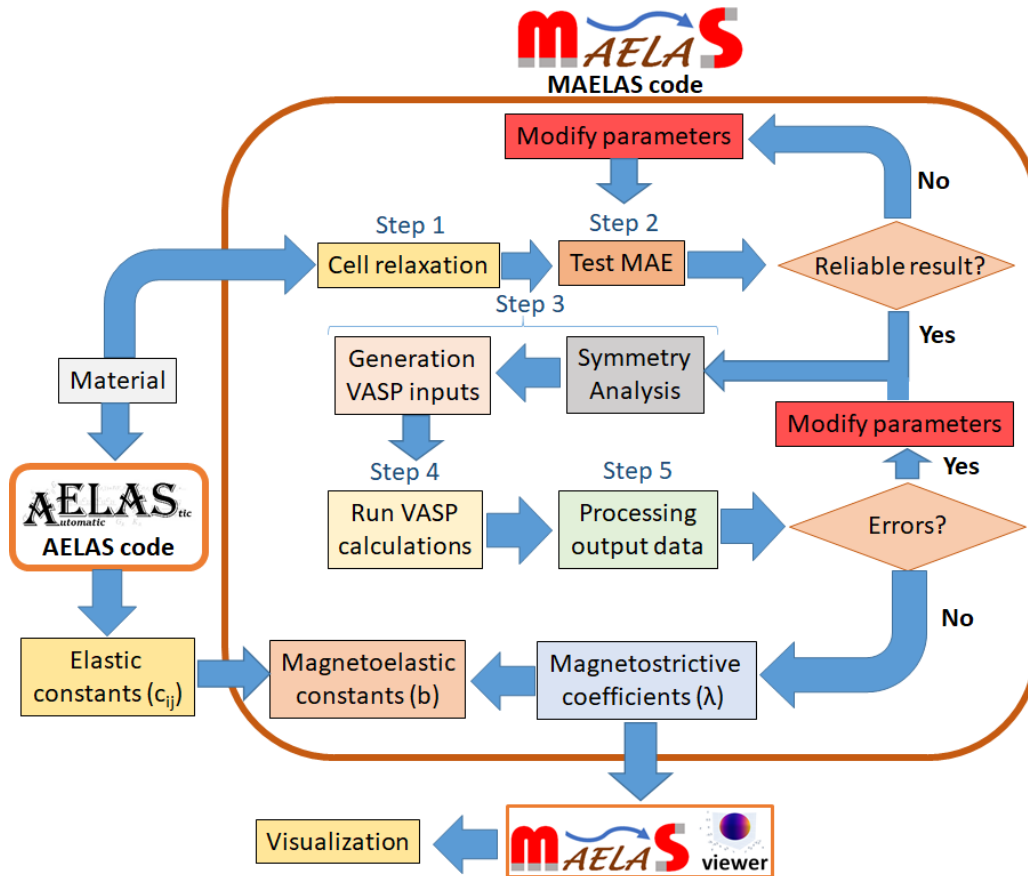
Figure 2: Workflow of the program MAELAS and its connection with the program AELAS [44].

with VASP code, which is an implementation of the projector augmented wave (PAW) method [55]. We use the interaction potentials generated for the Perdew-Burke-Ernzerhof (PBE) version [56] of the Generalized Gradient Approximation (GGA). We follow the recommended procedure to determine MAE with SOC included non-self-consistently. Namely, a first collinear spin-polarized job (without SOC) is performed to calculate the wavefunction and charge density, and then a second non-collinear spin-polarized job is performed in a non-self-consistent manner, by switching on the SOC, reading the wavefunction and charge density generated in the collinear job, and defining the spin orientation through the quantisation axis (SAXIS-tag) [57]. The number of bands included in the non-collinear job is set twice as large as the number of bands in the collinear job. By default, the code sets the tetrahedron method with Blöchl corrections for smearing

in the calculation of MAE. The energy convergence criterion of the electronic self-consistency was chosen as 10^{-9} eV/cell, while the force convergence criterion of ionic relaxation was used, with all forces acting on atoms being lower than 10^{-3} eV/Å. MAELAS also generates the input file with the set of k-points in the reciprocal space for VASP by using an automatic Monkhorst–Pack k-mesh [58] gamma-centered grid with length parameter R_k given by the user in the command line. Note the default settings generated by MAELAS for VASP might not work well for some materials, so that the user should check and tune them accordingly. For instance, in Section 4 we show some specific VASP settings and tests for few known materials. It is possible to use MAELAS with other codes instead of VASP, after file conversion to VASP format files. Although, this process might require some extra work for the user. For instance, we have recently made an interface between MAELAS and LAMMPS (spin-lattice simulations) [59–61].

4. Examples

In this section, we present some examples of the calculation of MAE, anisotropic magnetostrictive coefficients, elastic and magnetoelastic constants using MAE-LAS combined with AELAS [44] for a set of well-known magnetic materials. AELAS determines second-order elastic constants from the quadratic coefficients of the polynomial fitting of the energies versus strain relationships efficiently. For each material, we split the analysis into two parts. Firstly, we perform a cell relaxation, evaluate MAE and compute magnetostriction with MAELAS. In the second stage, we calculate the elastic constants with AELAS, and we use them as inputs to compute the magnetoelastic constants with MAELAS. To do so, we follow the workflow discussed in Section 3.2 (see Fig. 2). A summary of the results obtained in the following tests is shown in Tables 3, 4 and 5. All calculations correspond to zero-temperature.

Table 3: Anisotropic magnetostrictive coefficients and MAE calculated using the program MAE-LAS and measured in experiment ($T \approx 0$ K) for a set of magnetic materials. In parenthesis we show the magnetostrictive coefficients with Mason's definitions obtained using the relations given by Eq. A.2. These data correspond to the simulations with the largest number of k-points discussed in the main text.

Material	Crystal system	Method	Magnetostriction coefficient	MAELAS ($\times 10^{-6}$)	Expt. ($\times 10^{-6}$)	MAE	MAELAS (μeV/atom)	Expt. (μeV/atom)
FCC Ni	Cubic (I) SG 225	DFT GGA	λ_{001}	-78.4	-60^a	$E(110)-E(001)$	0.03	-2.15^b
			λ_{111}	-46.1	-35^a	$E(111)-E(001)$	0.34	-2.73^b
		SD-MD	λ_{001}	-61.9^h		$E(110)-E(001)$	-2.14^h	
			λ_{111}	-35.4^h		$E(111)-E(001)$	-2.86^h	
BCC Fe	Cubic (I) SG 229	DFT GGA	λ_{001}	25.7	26^a	$E(110)-E(001)$	0.24	1.0^b
			λ_{111}	17.2	-30^a	$E(111)-E(001)$	0.32	1.34^b
		SD-MD	λ_{001}	25.9^h		$E(110)-E(001)$	0.99^h	
			λ_{111}	-30.3^h		$E(111)-E(001)$	1.33^h	
HCP Co	Hexagonal (I) SG 194	DFT SCAN	$\lambda^{\alpha1,2}$ (λ_A)	85 (-78)	95 (-66)^c	$E(100)-E(001)$	53	61^b
			$\lambda^{\alpha2,2}$ (λ_B)	-115 (-92)	-126 (-123)^c			
			$\lambda^{\gamma,2}$ (λ_C)	15 (115)	57 (126)^c			
			$\lambda^{\varepsilon,2}$ (λ_D)	-19 (-1)	-286 (-128)^c			
		DFT LSDA+U $J=0.8$eV $U=3$eV	$\lambda^{\alpha1,2}$ (λ_A)	111 (-109)		$E(100)-E(001)$	58	
			$\lambda^{\alpha2,2}$ (λ_B)	-251 (-114)				
			$\lambda^{\gamma,2}$ (λ_C)	4 (251)				
			$\lambda^{\varepsilon,2}$ (λ_D)	-51 (10)				
YCo$_5$	Hexagonal (I) SG 191	DFT LSDA+U	$\lambda^{\alpha1,2}$	-90	$\|\lambda^{\alpha1,2}\|<100^d$	$E(100)-E(001)$	365	567^e
			$\lambda^{\alpha2,2}$	115	$\|\lambda^{\alpha2,2}\|<100^d$			
			$\lambda^{\gamma,2}$	76				
			$\lambda^{\varepsilon,2}$	141				
Fe$_2$Si	Trigonal (I) SG 164	DFT GGA	$\lambda^{\alpha1,2}$	-9		$E(100)-E(001)$	-38	
			$\lambda^{\alpha2,2}$	15				
			$\lambda^{\gamma,1}$	8				
			$\lambda^{\gamma,2}$	28				
			λ_{12}	-3				
			λ_{21}	-13				
L1$_0$ FePd	Tetragonal (I) SG 123	DFT GGA	$\lambda^{\alpha1,2}$	-21		$E(100)-E(001)$	106	181^f
			$\lambda^{\alpha2,2}$	79				
			$\lambda^{\gamma,2}$	31				
			$\lambda^{\varepsilon,2}$	28				
			$\lambda^{\delta,2}$	106				
			$\lambda^{\alpha1,0}-\frac{\lambda^{\alpha1,2}}{3}+\frac{\lambda^{\gamma,2}}{2}$		100^g			
YCo	Orthorhombic SG 63	DFT LSDA+U	λ_1	-11		$E(100)-E(001)$	22	
			λ_2	32		$E(010)-E(001)$	-23	
			λ_3	70				
			λ_4	-74				
			λ_5	-30				
			λ_6	7				
			λ_7	36				
			λ_8	-20				
			λ_9	35				

^{a}Ref.[40], ^{b}Ref.[62], ^{c}Ref.[63], ^{d}Ref.[7], ^{e}Ref.[64], ^{f}Ref.[65], ^{g}Ref.[66], ^{h}Ref.[59]

Table 4: Elastic and magnetoelastic constants calculated using the interface between AELAS and MAELAS codes. The third column shows the DFT method used to compute the elastic constants. The experimental elastic constants of FCC Ni and BCC Fe were measured at $T \approx 0$ K, while for HCP Co $T \approx 300$ K. The experimental magnetoelastic constants were estimated using the experimental elastic constants (seventh column) and the experimental magnetostrictive coefficients in Table 3 via the relations given in Section 2. The sixth column presents calculations of the elastic constants available in the Materials Project database [67, 68].

Material	Crystal system	Method	Elastic constant	AELAS (GPa)	Mat.Proj. (GPa)	Expt. (GPa)	Magnetoelastic constant	MAELAS (MPa)	Expt. (MPa)
FCC Ni	Cubic (I)	DFT GGA	C_{11}	298	276^g	261^h	b_1	15.5	9.9
	SG 225		C_{12}	166	159^g	151^h	b_2	19.4	13.9
			C_{44}	140	132^g	132^h			
		SD-MD	C_{11}	264^f			b_1	10.4	
			C_{12}	152^f			b_2	14.1	
			C_{44}	133^f					
BCC Fe	Cubic (I)	DFT GGA	C_{11}	288	247^a	243^b	b_1	-5.2	-4.1
	SG 229		C_{12}	152	150^a	138^b	b_2	-5.3	10.9
			C_{44}	104	97^a	122^b			
		SD-MD	C_{11}	230^f			b_1	-3.7	
			C_{12}	134^f			b_2	10.6	
			C_{44}	116^f					
HCP Co	Hexagonal (I)	DFT LSDA+U	C_{11}	327		307^d	b_{21}	-21.3	-31.9
	SG 194	$J = 0.8$eV	C_{12}	157		165^d	b_{22}	48.3	25.5
		$U = 3$eV	C_{13}	130		103^d	b_3	-0.7	-8.1
			C_{33}	308		358^d	b_4	7.1	42.9
			C_{44}	69		75^d			
		DFT SCAN	C_{11}	648			b_{21}	-51.3	
			C_{12}	212			b_{22}	40.5	
			C_{13}	189			b_3	6.4	
			C_{33}	633			b_4	8.9	
			C_{44}	239					
		DFT GGA	C_{11}		358^c				
			C_{12}		165^c				
			C_{13}		114^c				
			C_{33}		409^c				
			C_{44}		95^c				
YCo$_5$	Hexagonal (I)	DFT GGA	C_{11}	208	192^e		b_{21}	14.9	
	SG 191		C_{12}	103	123^e		b_{22}	-10.4	
			C_{13}	114	113^e		b_3	-8.0	
			C_{33}	270	262^e		b_4	-13.6	
			C_{44}	49	48^e				
		DFT LSDA+U	C_{11}	-63			b_{21}	13.9	
			C_{12}	363			b_{22}	-7.9	
			C_{13}	115			b_3	32.5	
			C_{33}	249			b_4	-12.4	
			C_{44}	44					

^{a}Ref.[69], ^{b}Ref.[70], ^{c}Ref.[71], ^{d}Ref.[72], ^{e}Ref.[73], ^{f}Ref.[59], ^{g}Ref.[74], ^{h}Ref.[75]

Table 5: Elastic and magnetoelastic constants calculated using the interface between AELAS and MAELAS codes. The third column shows the DFT method used to compute the elastic constants. The experimental elastic constants of $L1_0$ FePd were measured at $T \approx 300$ K. The sixth column presents calculations of the elastic constants available in the Materials Project database [67, 68].

Material	Crystal system	Method	Elastic constant	AELAS (GPa)	Mat.Proj. (GPa)	Expt. (GPa)	Magnetoelastic constant	MAELAS (MPa)	Expt. (MPa)
Fe_2Si	Trigonal (I) SG 164	DFT GGA	C_{11}	428	415^a		b_{21}	3.1	
			C_{12}	164	169^a		b_{22}	-4.2	
			C_{13}	133	133^a		b_3	-0.7	
			C_{14}	-27	-25^a		b_4	3.3	
			C_{33}	434	428^a		b_{14}	-1.4	
			C_{44}	118	107^a		b_{34}	-0.4	
$L1_0$ FePd	Tetragonal (I) SG 123	DFT GGA	C_{11}	324	293^b	214^c	b_{21}	-2.4	
			C_{12}	67	62^b	143^c	b_{22}	-15.2	
			C_{13}	133	125^b	143^c	b_3	-7.9	
			C_{33}	264	254^b	227^c	b'_3	-7.9	
			C_{44}	101	99^b	92^c	b_4	-5.6	
			C_{66}	37	38^b	93^c			
YCo	Orthorhombic SG 63	DFT GGA	C_{11}	76	94^d		b_1	-0.9	
			C_{12}	45	61^d		b_2	0.6	
			C_{13}	48	44^d		b_3	-5.0	
			C_{22}	102	93^d		b_4	5.7	
			C_{23}	55	56^d		b_5	0.9	
			C_{33}	141	121^d		b_6	1.5	
			C_{44}	40	38^d		b_7	-5.0	
			C_{55}	27	29^d		b_8	1.1	
			C_{66}	39	41^d		b_9	-8.2	
		DFT LSDA+U	C_{11}	101			b_1	-1.7	
			C_{12}	65			b_2	1.2	
			C_{13}	58			b_3	-3.8	
			C_{22}	94			b_4	4.3	
			C_{23}	70			b_5	-0.1	
			C_{33}	138			b_6	2.3	
			C_{44}	42			b_7	-4.4	
			C_{55}	29			b_8	1.1	
			C_{66}	35			b_9	-8.7	

[a]Ref.[76], [b]Ref.[77], [c]Ref.[78], [d]Ref.[79]

4.1. FCC Ni

In the first example, we consider FCC Ni, which is described by Eq.17 since it is a cubic (I) system.

4.1.1. Cell relaxation, MAE and magnetostrictive coefficients

Firstly, we perform a cell relaxation using an automatic k-point mesh with length parameter $R_k = 160$ centered on the Γ-point ($46 \times 46 \times 46$), 16 valence states, and energy cut-off 520 eV with PAW method and GGA-PBE. The relaxed lattice parameter is $a = 3.50419$ Å. Next, we analyze the dependence of

MAE and magnetostrictive coefficients on the k-point mesh ($R_k = 80$, 100, 120, 140 and 160) for this relaxed unit cell using the same VASP settings as in the cell relaxation. The results are shown in Fig. 3. We observe that $E(1,1,1) - E(0,0,1) > 0$ for all calculations up to 93150 k-points, while the experimental value is $-2.7 \mu eV$/atom [80]. This deviation may be due to the fact that we have not used a sufficiently large number of k-points, as Halilov et al. pointed out [80, 81]. Our results are in good agreement with the calculations performed by Trygg el at. where a similar number of k-points were used [82]. We also see that $E(1,1,1) - E(0,0,1)$ is approaching to negative values as the number of k-points is increased. Interestingly, the calculated magnetostrictive coefficients are in quite good agreement with the experimental ones [40] despite the deviation of MAE for the unstrained unit cell. One possible reason for this result may be that the calculation of the magnetostrictive coefficients involves larger energy difference between magnetization directions than the determination of MAE for the unstrained unit cell (which might be close to the accuracy limit of VASP $\sim \mu eV$), see Fig.4. Consequently, a k-point mesh with about 10^5 k-points may be sufficient to obtain reliable magnetostrictive coefficients for FCC Ni using GGA, although a much more dense k-mesh would be needed to obtain a reliable MAE for the unstrained unit cell [80, 81]. Note that these two properties come from the SOC, so that in general it would be highly desirable that the used method to calculate the energies describes well both MAE and magnetostriction. Recently, we developed a spin-lattice model within the framework of coupled spin and molecular dynamics (SD-MD) that reproduces accurately the experimental elastic and magnetoelastic energies at zero-temperature [59]. We obtained very good results by applying MAELAS to this coarse-grained model of SOC, see Tables 3 and 4.

4.1.2. Elastic and magnetoelastic constants

To compute the elastic constants we make use of AELAS code [44]. As inputs, we use the same relaxed cell and VASP settings as in the calculation of magnetostriction, but with lower number of k-points $R_k = 60$ ($17 \times 17 \times 17$ for the not distorted cell) and not including SOC. Once we have the elastic constants, we use them as inputs to derive the magnetoelastic constants with MAELAS. The results are shown in Table 4, where we also include calculations of elastic constants available in the Materials Project database [67, 68] and experimental data [75]. We observe that the value of $C_{11} = 298$ GPa obtained with GGA is higher than the one in the Materials Project $C_{11} = 276$ GPa and in the experiment $C_{11} = 261$ GPa. Concerning the magnetoelastic constants, we see that both b_1 and b_2 are in fairly good agreement with the experiment.
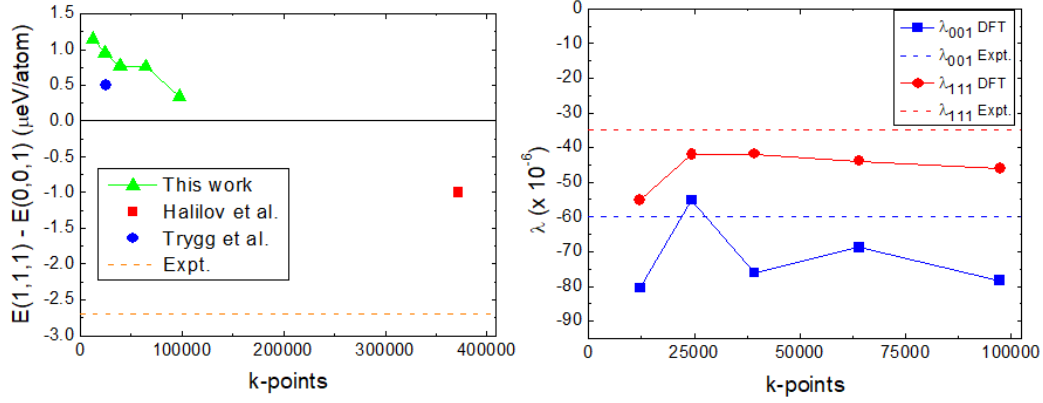
Figure 3: Calculation of (left) MAE of the unstrained unit cell and (right) magnetostrictive coefficients for FCC Ni as a function of k-points.
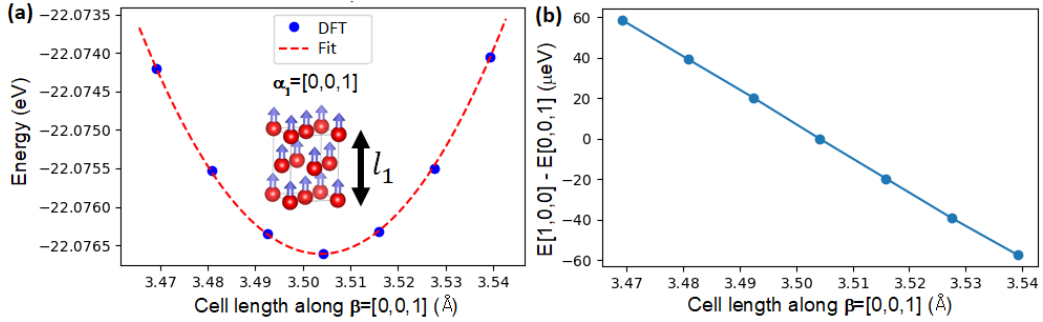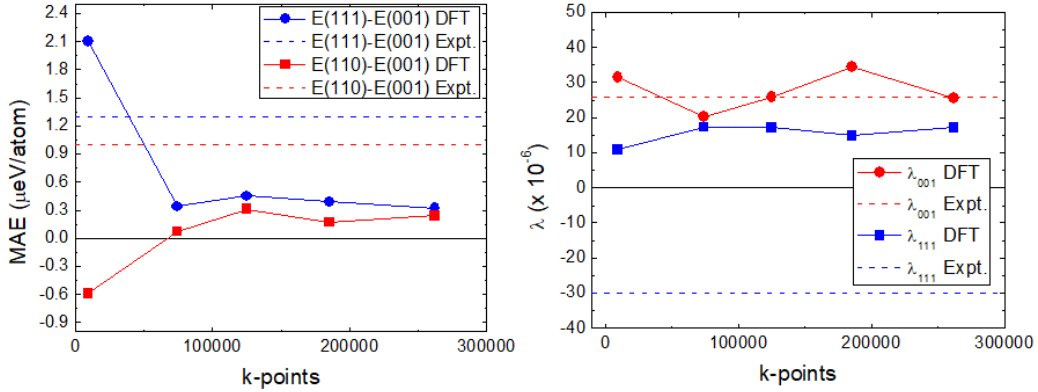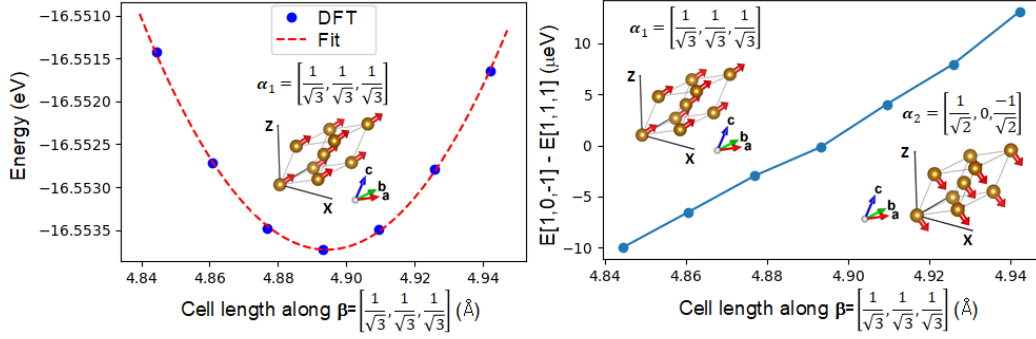

Figure 4: Calculation of λ_{001} for FCC Ni using MAELAS. (Left) Quadratic curve fit to the energy versus cell length along $\boldsymbol{\beta} = (0,0,1)$ with spin direction $\boldsymbol{\alpha}_1 = (0,0,1)$. (Right) Energy difference between states with spin directions $\boldsymbol{\alpha}_2 = (1,0,0)$ and $\boldsymbol{\alpha}_1 = (0,0,1)$ against the cell length along $\boldsymbol{\beta} = (0,0,1)$.

4.2. BCC Fe

In this example, we consider BCC Fe, which is described by Eq.17 since it is a cubic (I) system.

4.2.1. Cell relaxation, MAE and magnetostrictive coefficients

In the first stage, we we perform a cell relaxation for the conventional cubic unit cell of the BCC (2 atoms/cell) using a $57 \times 57 \times 57$ k-mesh with 185193 k-points in the Brillouin zone. The interactions were described by a PAW potential with 14 valence electrons within the PBE approximation to the exchange-correlation, and the PW basis was generated for an energy cut-off of 380 eV (30%

larger than the default value). The relaxed lattice parameter is $a = 2.82509$ Å. In Fig. 5 we show the dependence of MAE and magnetostriction on the k-points for this relaxed cell using the same exchange-correlation and energy cut-off as in the cell relaxation. The calculated values of MAE with the largest number of k-points (262144) are $E(110) - E(001) = 0.32 \mu$eV/atom and $E(111) - E(001) = 0.24 \mu$eV/atom which are a bit lower than the experimental values 1μeV/atom and 1.34μeV/atom, respectively [62]. Concerning the magnetostrictive coefficients, we obtained $\lambda_{001} = 25.7 \times 10^{-6}$ and $\lambda_{111} = 17.2 \times 10^{-6}$, while the experimental values at $T = 4.2$K are $\lambda_{001} = 26 \times 10^{-6}$ and $\lambda_{111} = -30 \times 10^{-6}$ [40]. We see that λ_{001} is quite close to the experimental result, while λ_{111} is in good agreement with previous DFT calculations [21, 25, 83] but it has the opposite sign as the experimental value. The calculation of λ_{111} is presented in Fig.6. We observe that the sign of the derivative of the energy difference between states with spin directions $\boldsymbol{\alpha}_2 = \left(\frac{1}{\sqrt{2}}, 0, \frac{-1}{\sqrt{2}} \right)$ and $\boldsymbol{\alpha}_1 = \left(\frac{1}{\sqrt{3}}, \frac{1}{\sqrt{3}}, \frac{1}{\sqrt{3}} \right)$ with respect to the cell length along $\boldsymbol{\beta} = \left(\frac{1}{\sqrt{3}}, \frac{1}{\sqrt{3}}, \frac{1}{\sqrt{3}} \right)$ evaluated at $l = l_2$ is equal to the sign of the calculated λ_{111} (> 0), as expected from Eq.52. However, the experimental λ_{111} is negative. This deviation might be due to a possible failure of GGA related to the location of the Fermi level in a region of majority band t2g density of states [84, 85]. Aiming to clarify the influence of MAELAS in this result, we applied MAELAS to a spin-lattice model for BCC Fe, that reproduces accurately the experimental elastic and magnetoelastic energies, obtaining almost the same experimentally observed magnetostriction [59], see Tables 3 and 4.

Figure 5: Calculation of (left) MAE of the unstrained unit cell and (right) magnetostrictive coefficients for BCC Fe as a function of k-points.

Figure 6: Calculation of λ_{111} for BCC Fe using MAELAS. (Left) Quadratic curve fit to the energy versus cell length along $\boldsymbol{\beta} = \left(\frac{1}{\sqrt{3}}, \frac{1}{\sqrt{3}}, \frac{1}{\sqrt{3}}\right)$ with spin direction $\boldsymbol{\alpha}_1 = \left(\frac{1}{\sqrt{3}}, \frac{1}{\sqrt{3}}, \frac{1}{\sqrt{3}}\right)$. (Right) Energy difference between states with spin directions $\boldsymbol{\alpha}_2 = \left(\frac{1}{\sqrt{2}}, 0, \frac{-1}{\sqrt{2}}\right)$ and $\boldsymbol{\alpha}_1 = \left(\frac{1}{\sqrt{3}}, \frac{1}{\sqrt{3}}, \frac{1}{\sqrt{3}}\right)$ against the cell length along $\boldsymbol{\beta} = \left(\frac{1}{\sqrt{3}}, \frac{1}{\sqrt{3}}, \frac{1}{\sqrt{3}}\right)$.

4.2.2. Elastic and magnetoelastic constants

As inputs for AELAS code [44], we use the same relaxed cell and VASP settings as in the calculation of magnetostriction, but with lower number of k-points $R_k = 60$ ($21 \times 21 \times 21$ for the not distorted cell) and not including SOC. Once we have the elastic constants, we use them as inputs to derive the magnetoelastic constants with MAELAS. The results are shown in Table 4, where we also include calculations of elastic constants available in the Materials Project database [67, 68] and experimental data [70]. We observe that the value of $C_{11} = 288$ GPa obtained with AELAS is significantly higher than the one in the Materials Project $C_{11} = 247$ GPa and in the experiment $C_{11} = 243$ GPa. Regarding the magnetoelastic constants, we see that the value for $b_1 = -5.2$ MPa generated with MAELAS is close to the estimated experimental value $b_1 = -4.1$ MPa. However, we obtain a negative sign for $b_2 = -5.4$ MPa, while in the experiment it is positive $b_2 = 10.9$ MPa. This deviation is due to the positive sign of λ_{111} given by DFT that we have mentioned above, see Eq.18 [25, 84, 85].

4.3. HCP Co

As a first example of hexagonal (I) system, we consider HCP Co.

4.3.1. Cell relaxation, MAE and magnetostrictive coefficients

For this material, we set the length parameter $R_k = 160$ for the generation of the automatic k-point mesh, which for the relaxed (not distorted) cell, results

in a $75\times75\times40$ k-point grid with 250000 points in the Brillouin zone. All calculations were done with an energy cut-off 406.563 eV (50% larger than the default one), 15 electrons in the valence states, and the meta-GGA functional SCAN [86], with aspherical contributions to the PAW one-centre terms. The relaxed lattice parameters are $a = b = 2.4561$ Å and $c = 3.9821$ Å. The calculated MAE for the relaxed cell is $E(100) - E(001) = 53\mu eV$/atom which is quite close to the experimental value $61\mu eV$/atom [62]. As it is shown in Table 3, the calculated magnetostrictive coefficients are also close to the experimental ones, except for $\lambda^{\varepsilon,2}$. Similarly, converting them into Mason's definitions via the relations given by Eq.A.2, we see that only $\lambda_D = -1 \times 10^{-6}$ is significantly deviated from the experiment (-128×10^{-6}) [63]. Aiming to clarify this result, we performed a direct calculation of λ_D using $\boldsymbol{\beta} = \left(\frac{1}{\sqrt{2}}, 0, \frac{1}{\sqrt{2}}\right)$, $\boldsymbol{\alpha}_1 = \left(\frac{1}{\sqrt{2}}, 0, \frac{1}{\sqrt{2}}\right)$ and $\boldsymbol{\alpha}_2 = (0,0,1)$ finding $\lambda_D = -9 \times 10^{-6}$, which is consistent with the indirect calculation through Clark's definition but still far from the experimental value. Fig.7 shows the quadratic curve fit to the energy versus cell length along $\boldsymbol{\beta} = (1,0,0)$ with $\boldsymbol{\alpha}_1 = \left(\frac{1}{\sqrt{3}}, \frac{1}{\sqrt{3}}, \frac{1}{\sqrt{3}}\right)$ to calculate $\lambda^{\alpha1,2}$.
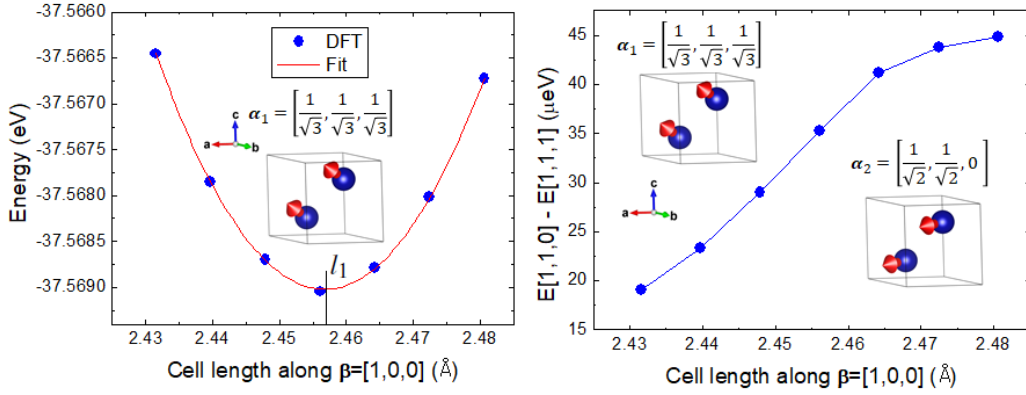
Figure 7: Calculation of $\lambda^{\alpha1,2}$ for HCP Co using MAELAS with the meta-GGA functional SCAN. (Left) Quadratic curve fit to the energy versus cell length along $\boldsymbol{\beta} = (1,0,0)$ with spin direction $\boldsymbol{\alpha}_1 = \left(\frac{1}{\sqrt{3}}, \frac{1}{\sqrt{3}}, \frac{1}{\sqrt{3}}\right)$. (Right) Energy difference between states with spin directions $\boldsymbol{\alpha}_2 = \left(\frac{1}{\sqrt{2}}, \frac{1}{\sqrt{2}}, 0\right)$ and $\boldsymbol{\alpha}_1 = \left(\frac{1}{\sqrt{3}}, \frac{1}{\sqrt{3}}, \frac{1}{\sqrt{3}}\right)$ against the cell length along $\boldsymbol{\beta} = (1,0,0)$.

We have also performed a second test using the rotationally invariant LSDA+U approach introduced by Liechtenstein et al. [87] fixing $J = 0.8$eV and varying U on the d-electrons [64]. In all calculations we use the same pseudopotential and

number of k-points as in the tests performed with SCAN. The energy cut-off is set to 380 eV. In this case the relaxed lattice parameters are $a = b = 2.48896$ Å and $c = 4.02347$ Å. The analysis of MAE and magnetostriction for different values of U is shown in Fig.8. We see that MAE approximates the experimental value at $U = 3$eV, so that we might expect a reliable description of SOC for this value of U. Increasing U up to 3eV has a significant effect on $\lambda^{\alpha 1,2}$ and $\lambda^{\alpha 2,2}$ making them to approach the experimental values. On the other hand, $\lambda^{\gamma,2}$ and $\lambda^{\varepsilon,2}$ don't change too much within the range of values used for U. The sign of all magnetostrictive coefficients are in good agreement to the experimental ones. However, as in the case with SCAN, $\lambda^{\varepsilon,2}$ is significantly underestimated. Possible reasons for this systematic deviation might be a failure of DFT [85], the applied deformations (we used the default value 0.01 for the tag $-s$ that sets the maximum value of parameter s in the generation of the deformed unit cells, see Eq.C.4), the used VASP settings (k-point mesh, exchange-correlation functional, smearing method, lattice parameters, ...) or higher order corrections in the equation of the relative length change Eq.25 [88]. This issue should be further investigated to clarify its possible causes.
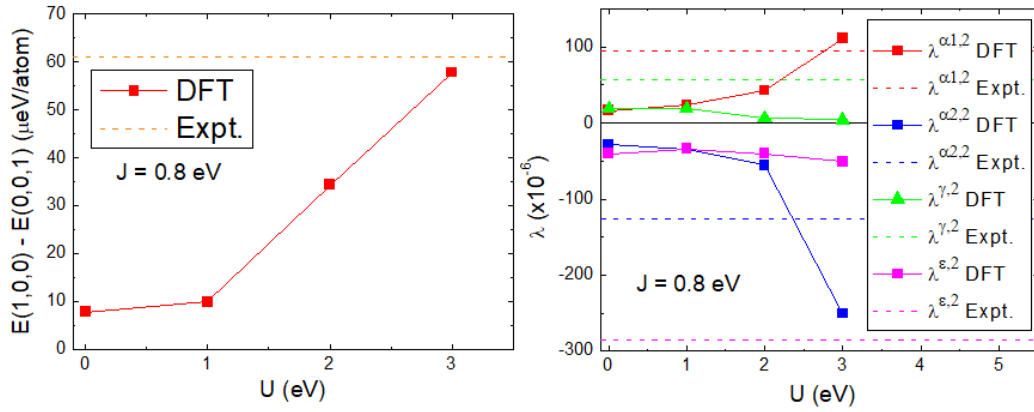
Figure 8: Calculation of (left) MAE of the unstrained unit cell and (right) magnetostrictive coefficients for HCP Co using the LSDA+U approach with different values of parameter U.

4.3.2. Elastic and magnetoelastic constants

For the calculation of the elastic constants we use the same relaxed cell and VASP settings as in the calculation of magnetostriction, but without SOC and lower number of k-points $R_k = 60$ ($28 \times 28 \times 15$ for the not distorted cell). In addition to SCAN, we also run calculations with LSDA+U setting $J = 0.8eV$

and $U = 3$eV. In Table 4, we see that LSDA+U and GGA (Materials Project database [74]) give better results than SCAN for both the elastic and magnetoelastic constants. The magnetoelastic constants obtained with LSDA+U are moderately good, except for b_3 and b_4 which are one order of magnitude lower than in the experiment, mainly due to the deviations coming from $\lambda^{\gamma,2}$ and $\lambda^{\varepsilon,2}$ given by MAELAS, see Table 3.

4.4. YCo$_5$

In this example we study the hexagonal (I) system YCo$_5$ with prototype CaCu$_5$ structure (space group 191).

4.4.1. Cell relaxation, MAE and magnetostrictive coefficients

We use the simplified (rotationally invariant) approach to the LSDA+U introduced by Dudarev et al. [89] with parameters $U = 1.9$ eV and $J = 0.8$ eV for Co, and $U = J = 0$ eV for Y given in Ref.[64]. For the calculation of the relaxed cell, MAE and magnetostrictive coefficients we used an automatic k-point mesh with length parameter $R_k = 100$ centered on the Γ-point ($23 \times 23 \times 25$ for the not distorted cell), 11 and 9 valence states for Y and Co, respectively, and energy cut-off 375 eV. The cell relaxation leads to lattice parameters $a = b = 4.9253$ Å and $c = 3.9269$ Å. The calculated MAE is $E(100) - E(001) = 365\mu$eV/atom which is lower than the experimental value 567μeV/atom [64]. Andreev measured the magnetostriction along a and c axis, finding that the magnitude of $|\lambda^{\alpha1,2}|$ and $|\lambda^{\alpha2,2}|$ can not be greater than 10^{-4} [7]. We obtained $\lambda^{\alpha1,2} = -90 \times 10^{-6}$ and $\lambda^{\alpha2,2} = 115 \times 10^{-6}$ which are quite close to the experimental upper limit. In Fig.9 we present the quadratic curve fit to the energy versus cell length along $\boldsymbol{\beta} = (0,0,1)$ with $\boldsymbol{\alpha}_1 = (0,0,1)$ to calculate $\lambda^{\alpha2,2}$.

4.4.2. Elastic and magnetoelastic constants

The calculation of the elastic constants is performed using the same relaxed cell and VASP settings as for magnetostriction, but without SOC and lower number of k-points $R_k = 60$ ($14 \times 14 \times 15$ for the not distorted cell). In addition to LSDA+U, we also run calculations with GGA. In Table 4, we observe that LSDA+U leads to an unstable phase ($C_{11} - C_{12} < 0$), while GGA gives better results.

4.5. Fe$_2$Si

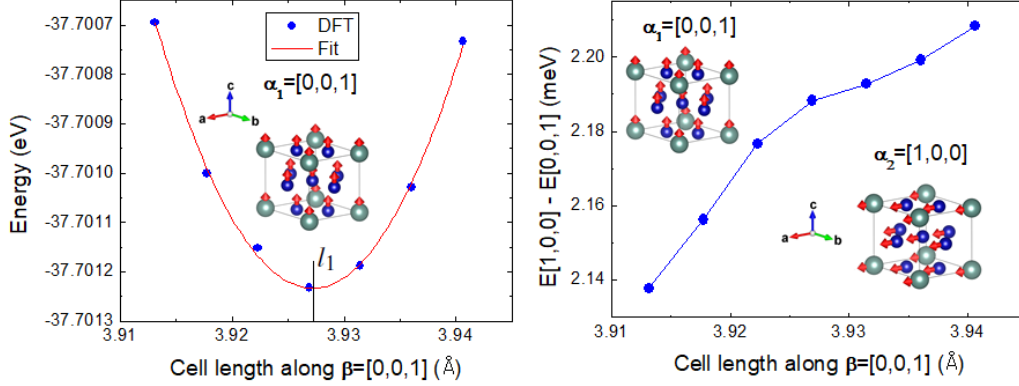To illustrate the application of MAELAS to trigonal (I) systems, we apply it to Fe$_2$Si (space group 164) [90].

34

Figure 9: Calculation of $\lambda^{\alpha 2,2}$ for YCo$_5$ using MAELAS. (Left) Quadratic curve fit to the energy versus cell length along $\boldsymbol{\beta} = (0,0,1)$ with spin direction $\boldsymbol{\alpha}_1 = (0,0,1)$. (Right) Energy difference between states with spin directions $\boldsymbol{\alpha}_2 = (1,0,0)$ and $\boldsymbol{\alpha}_1 = (0,0,1)$ against the cell length along $\boldsymbol{\beta} = (0,0,1)$.

4.5.1. Cell relaxation, MAE and magnetostrictive coefficients

For the calculation of the cell relaxation, MAE and magnetostrictive coefficients we used an automatic k-point mesh with length parameter $R_k = 80$ centered on the Γ-point ($24 \times 24 \times 17$ for the not distorted cell), 14 and 4 valence states for Fe and Si, respectively, and energy cut-off 520 eV with PAW method and GGA-PBE. The relaxed lattice parameters are $a = 3.9249$ Å and $c = 4.8311$ Å. The calculated MAE is $E(100) - E(001) = -38\mu$eV/atom (easy plane). Sun et al. reported MAE values with the screened hybrid Heyd-Scuseria-Ernzerhof (HSE06) functional smaller than with PBE for 2D Fe$_2$Si [91, 92]. Chi Pui Tang et al. calculated some electronic properties for bulk Fe$_2$Si finding that the densities of states in the vicinity of the Fermi level is mainly contributed from the d-electrons of Fe [93]. In Table 3, we observe that the overall anisotropic magnetostriction given by MAELAS is rather small, which makes this material interesting for high-flux core applications because it can reduce hysteresis loss [94].

4.5.2. Elastic and magnetoelastic constants

As inputs for AELAS, we use the same relaxed cell and VASP settings as in the calculation of magnetostriction, but without SOC and lower number of k-points $R_k = 60$ ($18 \times 18 \times 12$ for the not distorted cell). In Table 5, we see that AELAS gives similar elastic constants as in the Materials Project [76]. The derived magnetoelastic constants are small which is consistent with the low magnetostrictive coefficients that we obtained previously.
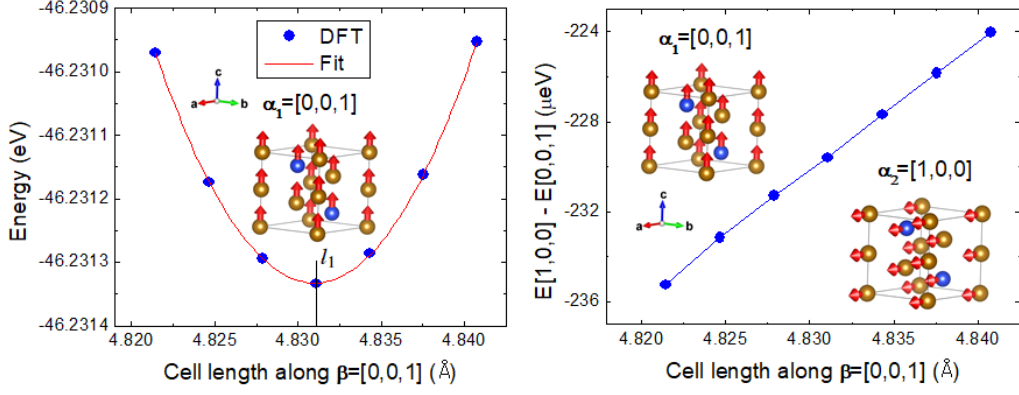
35

Figure 10: Calculation of $\lambda^{\alpha 2,2}$ for Fe$_2$Si using MAELAS. (Left) Quadratic curve fit to the energy versus cell length along $\boldsymbol{\beta} = (0,0,1)$ with spin direction $\boldsymbol{\alpha}_1 = (0,0,1)$. (Right) Energy difference between states with spin directions $\boldsymbol{\alpha}_2 = (1,0,0)$ and $\boldsymbol{\alpha}_1 = (0,0,1)$ against the cell length along $\boldsymbol{\beta} = (0,0,1)$.

4.6. L1$_0$ FePd

As an example of tetragonal (I) system, we calculate the anisotropic magnetostrictive coefficients of L1$_0$ FePd (space group 123).

4.6.1. Cell relaxation, MAE and magnetostrictive coefficients

For the calculation of the cell relaxation, MAE and magnetostrictive coefficients we used an automatic k-point mesh with length parameter $R_k = 100$ centered on the Γ-point ($37 \times 37 \times 27$ for the not distorted cell), 8 and 10 valence states for Fe and Pd, respectively, and energy cut-off 375 eV with PAW method and GGA-PBE. The relaxed lattice parameters are $a = 2.6973$ Å and $c = 3.7593$ Å. We obtained a MAE $E(100) - E(001) = 106 \mu$eV/atom which is lower than in the experiment 181μeV/atom [65]. The values of the obtained anisotropic magnetostrictive coefficients are shown in Table 3. Shima et al. reported a relative length change equal to 100×10^{-6} along a-axis under a magnetic field in the same direction ($\boldsymbol{\beta} = \boldsymbol{\alpha} = (1,0,0)$) [66]. According to Eq.40, this measurement corresponds to $\lambda^{\alpha 1,0} - \frac{\lambda^{\alpha 1,2}}{3} + \frac{\lambda^{\gamma,2}}{2}$. For the anisotropic part of this quantity, we obtained $-\frac{\lambda^{\alpha 1,2}}{3} + \frac{\lambda^{\gamma,2}}{2} = 22.5 \times 10^{-6}$. In Fig.11 we show the quadratic curve fit to the energy versus cell length along $\boldsymbol{\beta} = (1,0,0)$ with $\boldsymbol{\alpha}_1 = (1,0,0)$ to calculate $\lambda^{\gamma,2}$.
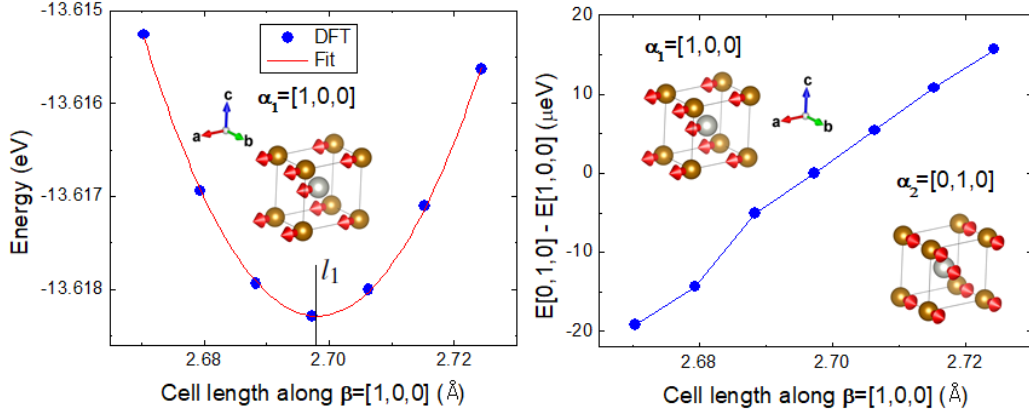
Figure 11: Calculation of $\lambda^{\gamma,2}$ for $L1_0$ FePd using MAELAS. (Left) Quadratic curve fit to the energy versus cell length along $\boldsymbol{\beta} = (1,0,0)$ with spin direction $\boldsymbol{\alpha}_1 = (1,0,0)$. (Right) Energy difference between states with spin directions $\boldsymbol{\alpha}_2 = (0,1,0)$ and $\boldsymbol{\alpha}_1 = (1,0,0)$ versus the cell length along $\boldsymbol{\beta} = (1,0,0)$.

4.6.2. Elastic and magnetoelastic constants

The calculation of the elastic constants with AELAS is performed using the same relaxed cell and VASP settings as for magnetostriction, but without SOC and lower number of k-points $R_k = 60$ ($22 \times 22 \times 16$ for the not distorted cell). As we see in Table 5, we obtain similar results as in the Materials Project database [77].

4.7. YCo

For the case of orthorhombic systems, we study the compound YCo (space group 63) [95].

4.7.1. Cell relaxation, MAE and magnetostrictive coefficients

In this case, we use the simplified (rotationally invariant) approach to the LSDA+U [89] with parameters $U = 1.9$ eV and $J = 0.8$ eV for Co, and $U = J = 0$ eV for Y in the same way as in YCo_5 [64]. For the calculation of the relaxed cell, MAE and magnetostrictive coefficients we used an automatic k-point mesh with length parameter $R_k = 90$ centered on the Γ-point ($22 \times 9 \times 23$ for the not distorted cell), 11 and 9 valence states for Y and Co, respectively, and energy cut-off 375 eV. The cell relaxation leads to lattice parameters $a = 4.0686$ Å, $b = 10.3157$ Å and $c = 3.8957$ Å. As we see in Table 3, both MAE and magnetostriction are quite small for this material.
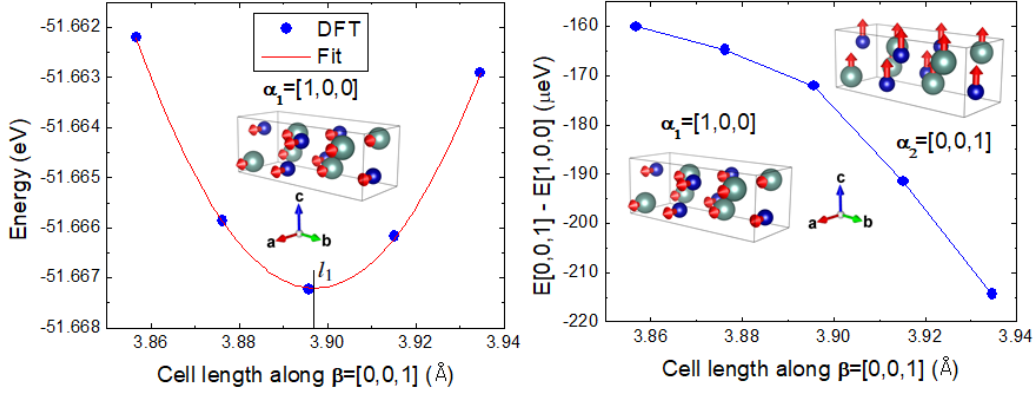
Figure 12: Calculation of λ_5 for YCo using MAELAS. (Left) Quadratic curve fit to the energy versus cell length along $\boldsymbol{\beta} = (0,0,1)$ with spin direction $\boldsymbol{\alpha}_1 = (1,0,0)$. (Right) Energy difference between states with spin directions $\boldsymbol{\alpha}_2 = (0,0,1)$ and $\boldsymbol{\alpha}_1 = (1,0,0)$ against the cell length along $\boldsymbol{\beta} = (0,0,1)$.

4.7.2. *Elastic and magnetoelastic constants*

The calculation of the elastic constants is performed using the same relaxed cell and VASP settings as for magnetostriction, but without SOC and lower number of k-points $R_k = 60$ ($15 \times 6 \times 15$ for the not distorted cell). In addition to LSDA+U, we also run calculations with GGA. In Table 5, we observe that both LSDA+U and GGA lead to similar elastic and magnetoelastic constants.

5. Conclusions and future perspectives

In summary, the program MAELAS offers computational tools to tackle the complex phenomenon of magnetostriction by automated first-principles calculations. It could potentially be used to discover and design novel magnetostrictive materials by a high-throughput screening approach. In particular, materials with giant magnetostriction (beyond conventional cubic and hexagonal systems), isotropic or very low magnetostriction (like FeNi alloys) might be of technological importance.

The preliminary tests of the program show quite encouraging results, although there is still room for improvement. First principle calculations are still quite challenging for materials with very low MAE or localized 4f-electrons [64]. In this sense, MAELAS could also be a useful tool to understand, test and improve the DFT methods to compute induced properties by SOC and crystal field interactions like the MAE of unstrained systems and anisotropic magnetostriction.

Presently, we are working on new features of MAELAS and online visualization tools [51]. We are also considering to increase the number of supported crystal systems, as well as to implement more computationally efficient methods to calculate magnetoelastic constants and magnetostrictive coefficients. These extensions might be included in new versions of the code.

Acknowledgement

Appendix A. Conversion between different definitions of magnetostrictive coefficients for hexagonal (I)

The magnetostrictive coefficients for hexagonal (I) shown in Eq.25 were defined by Clark et al. in 1965 [16]. However, one can find other definitions like those given by Mason [15], Birss [34], and Callen and Callen [17]. In this appendix, we show the conversion formulas between these definitions and those provided by Clark et al. [16] (Eq.25).

Appendix A.1. Mason's form

In 1954, based on a general thermodynamic function with stresses and intensity of magnetization as the fundamental variables [96], Mason derived the

following form of the relative length change [15]

$$\frac{\Delta l}{l_0}\bigg|_{\boldsymbol{\beta}}^{\boldsymbol{\alpha}} = \lambda_{Mason}^{\alpha1,0}(\beta_x^2 + \beta_y^2) + \lambda_{Mason}^{\alpha2,0}\beta_z^2 + \lambda_A[(\alpha_x\beta_x + \alpha_y\beta_y)^2 - (\alpha_x\beta_x + \alpha_y\beta_y)\alpha_z\beta_z]$$

$$+ \lambda_B[(1 - \alpha_z^2)(1 - \beta_z^2) - (\alpha_x\beta_x + \alpha_y\beta_y)^2]$$
$$+ \lambda_C[(1 - \alpha_z^2)\beta_z^2 - (\alpha_x\beta_x + \alpha_y\beta_y)\alpha_z\beta_z] + 4\lambda_D(\alpha_x\beta_x + \alpha_y\beta_y)\alpha_z\beta_z.$$

(A.1)

These magnetostrictive coefficients are related to those defined in Eq.25 as [16]

$$\lambda_{Mason}^{\alpha1,0} = \lambda^{\alpha1,0} + \frac{2}{3}\lambda^{\alpha1,2}$$

$$\lambda_{Mason}^{\alpha2,0} = \lambda^{\alpha2,0} + \frac{2}{3}\lambda^{\alpha2,2}$$

$$\lambda_A = -\lambda^{\alpha1,2} + \frac{1}{2}\lambda^{\gamma,2}$$

$$\lambda_B = -\lambda^{\alpha1,2} - \frac{1}{2}\lambda^{\gamma,2}$$

$$\lambda_C = -\lambda^{\alpha2,2}$$

$$\lambda_D = \frac{1}{2}\lambda^{\epsilon,2} - \frac{1}{4}\lambda^{\alpha1,2} + \frac{1}{8}\lambda^{\gamma,2} - \frac{1}{4}\lambda^{\alpha2,2}.$$

(A.2)

Note in the original work of Mason [15] the terms that describes the volume magnetostriction were not included. Here we added these terms ($\lambda_{Mason}^{\alpha1,0}$, $\lambda_{Mason}^{\alpha2,0}$) in order to fully recover the Eq.25.

Appendix A.2. Birss's form

In 1959 Birss derived an equivalent equation of relative length change in this form [34]

$$\frac{\Delta l}{l_0}\bigg|_{\boldsymbol{\beta}}^{\boldsymbol{\alpha}} = Q_0 + Q_1\beta_z^2 + Q_2(1 - \alpha_z^2) + Q_4(1 - \alpha_z^2)\beta_z^2 + Q_6(\alpha_x\beta_x + \alpha_y\beta_y)\alpha_z\beta_z$$

$$+ Q_8(\alpha_x\beta_x + \alpha_y\beta_y)^2.$$

(A.3)

40

These magnetostrictive coefficients are related to those defined in Eq.25 as [16]

$$Q_0 = \lambda^{\alpha 1,0} + \frac{2}{3}\lambda^{\alpha 1,2}$$

$$Q_1 = \lambda^{\alpha 2,0} + \frac{2}{3}\lambda^{\alpha 2,2} - \lambda^{\alpha 1,0} - \frac{2}{3}\lambda^{\alpha 1,2}$$

$$Q_2 = -\lambda^{\alpha 1,2} - \frac{1}{2}\lambda^{\gamma,2}$$

$$Q_4 = \lambda^{\alpha 1,2} + \frac{1}{2}\lambda^{\gamma,2} - \lambda^{\alpha 2,2} \tag{A.4}$$

$$Q_6 = 2\lambda^{\varepsilon,2}$$

$$Q_8 = \lambda^{\gamma,2}.$$

Appendix A.3. Callen and Callen's form

In 1965 Callen and Callen obtained other equivalent form of the equation of relative length change by including two-ion interactions into the theory of magnetostriction arising from single-ion crystal-field effects [17]. It reads

$$\left.\frac{\Delta l}{l_0}\right|_{\beta}^{\alpha} = \frac{1}{3}\lambda_{11}^{\alpha} + \frac{1}{2\sqrt{3}}\lambda_{12}^{\alpha}\left(\alpha_z^2 - \frac{1}{3}\right) + 2\lambda_{21}^{\alpha}\left(\beta_z^2 - \frac{1}{3}\right)$$
$$+ \sqrt{3}\lambda_{22}^{\alpha}\left(\alpha_z^2 - \frac{1}{3}\right)\left(\beta_z^2 - \frac{1}{3}\right) + \lambda^{\gamma}\left[\frac{1}{2}(\alpha_x^2 - \alpha_y^2)(\beta_x^2 - \beta_y^2) + 2\alpha_x\alpha_y\beta_x\beta_y\right]$$
$$+ 2\lambda^{\varepsilon}(\alpha_x\alpha_z\beta_x\beta_z + \alpha_y\alpha_z\beta_y\beta_z), \tag{A.5}$$

These magnetostrictive coefficients are related to those defined in Eq.25 as [17]

$$\lambda_{11}^{\alpha} = 2\lambda^{\alpha 1,0} + \lambda^{\alpha 2,0} + 2\lambda^{\alpha 1,2} + \lambda^{\alpha 2,2}$$

$$\lambda_{12}^{\alpha} = \frac{4}{\sqrt{3}}\lambda^{\alpha 1,2} + \frac{2}{\sqrt{3}}\lambda^{\alpha 2,2}$$

$$\lambda_{21}^{\alpha} = -\frac{1}{2}\lambda^{\alpha 1,0} + \frac{1}{2}\lambda^{\alpha 2,0}$$

$$\lambda_{22}^{\alpha} = -\frac{1}{\sqrt{3}}\lambda^{\alpha 1,2} + \frac{1}{\sqrt{3}}\lambda^{\alpha 2,2} \tag{A.6}$$

$$\lambda^{\varepsilon} = \lambda^{\varepsilon,2}$$

$$\lambda^{\gamma} = \lambda^{\gamma,2}.$$

Appendix B. Conversion between different definitions of magnetostrictive coefficients for tetragonal (I)

In 1994 Cullen et al. [8] derived the equation of relative length change given by Eq.40 for tetragonal (I) system. In 1954 Mason obtained an equivalent equation that reads [15]

$$
\left.\frac{\Delta l}{l_0}\right|_{\beta}^{\alpha} = \lambda_{Mason}^{\alpha 1,0}(\beta_x^2 + \beta_y^2) + \lambda_{Mason}^{\alpha 2,0}\beta_z^2 + \frac{1}{2}\lambda_1[(\alpha_x\beta_x - \alpha_y\beta_y)^2 - (\alpha_x\beta_y + \alpha_y\beta_x)^2
$$

$$
+ (1 - \beta_z^2)(1 - \alpha_z^2) - 2\alpha_z\beta_z(\alpha_x\beta_x + \alpha_y\beta_y)] + 4\lambda_2\alpha_z\beta_z(\alpha_x\beta_x + \alpha_y\beta_y)
$$

$$
+ 4\lambda_3\alpha_x\alpha_y\beta_x\beta_y + \lambda_4[\beta_z^2(1 - \alpha_z^2) - \alpha_z\beta_z(\alpha_x\beta_x + \alpha_y\beta_y)]
$$

$$
+ \frac{1}{2}\lambda_5[(\alpha_x\beta_y - \alpha_y\beta_x)^2 - (\alpha_x\beta_x + \alpha_y\beta_y)^2 + (1 - \beta_z^2)(1 - \alpha_z^2)].
$$

$$(B.1)$$

These magnetostrictive coefficients are related to those defined by Eq.40 in the following way

$$
\lambda_{Mason}^{\alpha 1,0} = \lambda^{\alpha 1,0} + \frac{2}{3}\lambda^{\alpha 1,2}
$$

$$
\lambda_{Mason}^{\alpha 2,0} = \lambda^{\alpha 2,0} + \frac{2}{3}\lambda^{\alpha 2,2}
$$

$$
\lambda_1 = -\lambda^{\alpha 1,2} + \frac{1}{2}\lambda^{\gamma,2}
$$

$$
\lambda_2 = \frac{1}{2}\lambda^{\varepsilon,2} - \frac{1}{4}\lambda^{\alpha 2,2} - \frac{1}{4}\lambda^{\alpha 1,2} + \frac{1}{8}\lambda^{\gamma,2}
$$

$$
\lambda_3 = \frac{1}{2}\lambda^{\delta,2} - \lambda^{\alpha 1,2}
$$

$$
\lambda_4 = -\lambda^{\alpha 2,2}
$$

$$
\lambda_5 = -\lambda^{\alpha 1,2} - \frac{1}{2}\lambda^{\gamma,2}.
$$

$$(B.2)$$

Note in the original work of Mason [15] the terms that describes the volume magnetostriction were not included. Here we added these terms ($\lambda_{Mason}^{\alpha 1,0}$, $\lambda_{Mason}^{\alpha 2,0}$) in order to fully recover the Eq.40.

Appendix C. Generation of the deformed unit cells

In this appendix we present the procedure to generate the deformed unit cells for the calculation of each magnetostrictive coefficient. The deformed unit cells

are generated by multiplying the lattice vectors of the initial unit cell $\boldsymbol{a} = (a_x, a_y, a_z)$, $\boldsymbol{b} = (b_x, b_y, b_z)$, $\boldsymbol{c} = (c_x, c_y, c_z)$ by the deformation gradient F_{ij} [97]

$$\begin{pmatrix} a'_x & b'_x & c'_x \\ a'_y & b'_y & c'_y \\ a'_z & b'_z & c'_z \end{pmatrix} = \begin{pmatrix} F_{xx} & F_{xy} & F_{xz} \\ F_{yx} & F_{yy} & F_{yz} \\ F_{zx} & F_{zy} & F_{zz} \end{pmatrix} \cdot \begin{pmatrix} a_x & b_x & c_x \\ a_y & b_y & c_y \\ a_z & b_z & c_z \end{pmatrix} \tag{C.1}$$

where a'_i, b'_i and c'_i ($i = x, y, z$) are the components of the lattice vectors of the deformed cell. In the infinitesimal strain theory, the deformation gradient is related to the displacement gradient ($\partial u_i / \partial r_j$) as $F_{ij} = \delta_{ij} + \partial u_i / \partial r_j$, where δ_{ij} is the Kronecker delta. Hence, according to Eq.5, the strain tensor ε_{ij} can be written in terms of the deformation gradient as

$$\boldsymbol{\varepsilon} = \begin{pmatrix} \varepsilon_{xx} & \varepsilon_{xy} & \varepsilon_{xz} \\ \varepsilon_{yx} & \varepsilon_{yy} & \varepsilon_{yz} \\ \varepsilon_{zx} & \varepsilon_{zy} & \varepsilon_{zz} \end{pmatrix} = \frac{1}{2} \begin{pmatrix} 2(F_{xx} - 1) & F_{xy} + F_{yx} & F_{xz} + F_{zx} \\ F_{xy} + F_{yx} & 2(F_{yy} - 1) & F_{yz} + F_{zy} \\ F_{xz} + F_{zx} & F_{yz} + F_{zy} & 2(F_{zz} - 1) \end{pmatrix}. \tag{C.2}$$

In MAELAS, we consider deformation gradients to optimize the unit cell in the measuring directions $\boldsymbol{\beta}$ given by Table 2. Additionally, we also constrain the determinant of the deformation gradients to be equal to one ($det(\boldsymbol{F}) = 1$) in order to preserve the volume of the unit cells (isochoric deformation) [21, 98]. We point out that there are other possible variants of the following deformation modes [85].

Appendix C.1. Cubic (I) system

For cubic (I) systems MAELAS generates two set of deformed unit cells with tetragonal deformations along $\boldsymbol{\beta} = (0, 0, 1)$ and trigonal deformations along $\boldsymbol{\beta} = (1/\sqrt{3}, 1/\sqrt{3}, 1/\sqrt{3})$ to calculate λ_{001} and λ_{111}, respectively (see Table 2). The deformation gradients for these two deformation modes are

$$\boldsymbol{F}^{\lambda_{001}}_{\boldsymbol{\beta}=(0,0,1)}(s) = \begin{pmatrix} \frac{1}{\sqrt{1+s}} & 0 & 0 \\ 0 & \frac{1}{\sqrt{1+s}} & 0 \\ 0 & 0 & 1+s \end{pmatrix}, \quad \boldsymbol{F}^{\lambda_{111}}_{\boldsymbol{\beta}=\left(\frac{1}{\sqrt{3}}, \frac{1}{\sqrt{3}}, \frac{1}{\sqrt{3}}\right)}(s) = \zeta \begin{pmatrix} 1 & \frac{s}{2} & \frac{s}{2} \\ \frac{s}{2} & 1 & \frac{s}{2} \\ \frac{s}{2} & \frac{s}{2} & 1 \end{pmatrix} \tag{C.3}$$

where $\zeta = \sqrt[3]{4/(4 - 3s^2 + s^3)}$. The parameter s controls the applied deformation, and its maximum value can be specified through the command line of the program MAELAS using tag $-s$. The total number of deformed cells can be chosen with tag $-n$.

Appendix C.2. Hexagonal (I) system

In the case of hexagonal (I), MAELAS generates 4 sets of deformed cells using the following deformation gradients

$$
\boldsymbol{F}\Big|^{\lambda^{\alpha 1,2}}_{\boldsymbol{\beta}=(1,0,0)}(s) = \begin{pmatrix} 1+s & 0 & 0 \\ 0 & \frac{1}{\sqrt{1+s}} & 0 \\ 0 & 0 & \frac{1}{\sqrt{1+s}} \end{pmatrix}, \boldsymbol{F}\Big|^{\lambda^{\alpha 2,2}}_{\boldsymbol{\beta}=(0,0,1)}(s) = \begin{pmatrix} \frac{1}{\sqrt{1+s}} & 0 & 0 \\ 0 & \frac{1}{\sqrt{1+s}} & 0 \\ 0 & 0 & 1+s \end{pmatrix}
$$

$$
\boldsymbol{F}\Big|^{\lambda^{\gamma,2}}_{\boldsymbol{\beta}=(1,0,0)}(s) = \begin{pmatrix} 1+s & 0 & 0 \\ 0 & \frac{1}{\sqrt{1+s}} & 0 \\ 0 & 0 & \frac{1}{\sqrt{1+s}} \end{pmatrix}, \boldsymbol{F}\Big|^{\lambda^{\varepsilon,2}}_{\boldsymbol{\beta}=\frac{(a,0,c)}{\sqrt{a^2+c^2}}}(s) = \omega \begin{pmatrix} 1 & 0 & \frac{sc}{2a} \\ 0 & 1 & 0 \\ \frac{sa}{2c} & 0 & 1 \end{pmatrix}
$$

$$\tag{C.4}$$

where $\omega = \sqrt[3]{4/(4-s^2)}$, a and c are the lattice parameters of the relaxed (not deformed) unit cell. The fractions c/a and a/c were introduced in the deformation gradient elements $F^{\lambda^{\varepsilon,2}}_{xz}$ and $F^{\lambda^{\varepsilon,2}}_{zx}$, respectively, in order to generate deformations that meet the property $\boldsymbol{\beta} = \frac{\boldsymbol{a}+\boldsymbol{c}}{|\boldsymbol{a}+\boldsymbol{c}|} = \frac{\boldsymbol{a}'+\boldsymbol{c}'}{|\boldsymbol{a}'+\boldsymbol{c}'|}$, where $\boldsymbol{a}'$ and $\boldsymbol{c}'$ are the lattice vectors of the distorted unit cell, see Fig. C.13. This deformation mode makes it easy to compute the cell length l in the measuring direction $\boldsymbol{\beta}$ since it is just $l = |\boldsymbol{a}' + \boldsymbol{c}'|$. It is inspired by the trigonal deformation for the cubic (I) case $\boldsymbol{F}^{\lambda_{111}}$ where deformations meet the property $\boldsymbol{\beta} = \frac{\boldsymbol{a}+\boldsymbol{b}+\boldsymbol{c}}{|\boldsymbol{a}+\boldsymbol{b}+\boldsymbol{c}|} = \frac{\boldsymbol{a}'+\boldsymbol{b}'+\boldsymbol{c}'}{|\boldsymbol{a}'+\boldsymbol{b}'+\boldsymbol{c}'|}$.
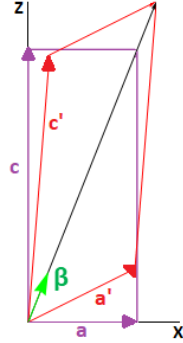

Figure C.13: Sketch of the deformation generated by the deformation gradient $\boldsymbol{F}^{\lambda^{\varepsilon,2}}$ given by Eq.C.4 to calculate $\lambda^{\varepsilon,2}$. The purple line represents the relaxed cell with lattice parameters (a,b,c), while the red line stands for the deformed cell with lattice parameters (a',b',c'). This deformation meets the property $\boldsymbol{\beta} = \frac{\boldsymbol{a}+\boldsymbol{c}}{|\boldsymbol{a}+\boldsymbol{c}|} = \frac{\boldsymbol{a}'+\boldsymbol{c}'}{|\boldsymbol{a}'+\boldsymbol{c}'|}$.

Appendix C.3. Trigonal (I) system

In the case of trigonal (I), MAELAS generates 6 sets of deformed unit cells using the following deformation gradients

$$\mathbf{F}\Big|_{\boldsymbol{\beta}=(1,0,0)}^{\lambda^{\alpha1,2}}(s) = \begin{pmatrix} 1+s & 0 & 0 \\ 0 & \frac{1}{\sqrt{1+s}} & 0 \\ 0 & 0 & \frac{1}{\sqrt{1+s}} \end{pmatrix}, \mathbf{F}\Big|_{\boldsymbol{\beta}=(0,0,1)}^{\lambda^{\alpha2,2}}(s) = \begin{pmatrix} \frac{1}{\sqrt{1+s}} & 0 & 0 \\ 0 & \frac{1}{\sqrt{1+s}} & 0 \\ 0 & 0 & 1+s \end{pmatrix}$$

$$\mathbf{F}\Big|_{\boldsymbol{\beta}=(1,0,0)}^{\lambda^{\gamma,1}}(s) = \begin{pmatrix} 1+s & 0 & 0 \\ 0 & \frac{1}{\sqrt{1+s}} & 0 \\ 0 & 0 & \frac{1}{\sqrt{1+s}} \end{pmatrix}$$

$$\mathbf{F}\Big|_{\boldsymbol{\beta}=\frac{(a,0,c)}{\sqrt{a^2+c^2}}}^{\lambda^{\gamma,2}}(s) = \mathbf{F}\Big|_{\boldsymbol{\beta}=\frac{(a,0,c)}{\sqrt{a^2+c^2}}}^{\lambda_{12}}(s) = \mathbf{F}\Big|_{\boldsymbol{\beta}=\frac{(a,0,c)}{\sqrt{a^2+c^2}}}^{\lambda_{21}}(s) = \omega \begin{pmatrix} 1 & 0 & \frac{sc}{2a} \\ 0 & 1 & 0 \\ \frac{sa}{2c} & 0 & 1 \end{pmatrix}.$$

$$\tag{C.5}$$

Appendix C.4. Tetragonal (I) system

In the case of tetragonal (I), MAELAS generates 5 sets of deformed cells using the following deformation gradients

$$\mathbf{F}\Big|_{\boldsymbol{\beta}=(1,0,0)}^{\lambda^{\alpha1,2}}(s) = \begin{pmatrix} 1+s & 0 & 0 \\ 0 & \frac{1}{\sqrt{1+s}} & 0 \\ 0 & 0 & \frac{1}{\sqrt{1+s}} \end{pmatrix}, \mathbf{F}\Big|_{\boldsymbol{\beta}=(0,0,1)}^{\lambda^{\alpha2,2}}(s) = \begin{pmatrix} \frac{1}{\sqrt{1+s}} & 0 & 0 \\ 0 & \frac{1}{\sqrt{1+s}} & 0 \\ 0 & 0 & 1+s \end{pmatrix}$$

$$\mathbf{F}\Big|_{\boldsymbol{\beta}=(1,0,0)}^{\lambda^{\gamma,2}}(s) = \begin{pmatrix} 1+s & 0 & 0 \\ 0 & \frac{1}{\sqrt{1+s}} & 0 \\ 0 & 0 & \frac{1}{\sqrt{1+s}} \end{pmatrix}, \mathbf{F}\Big|_{\boldsymbol{\beta}=\frac{(a,0,c)}{\sqrt{a^2+c^2}}}^{\lambda^{\varepsilon,2}}(s) = \omega \begin{pmatrix} 1 & 0 & \frac{sc}{2a} \\ 0 & 1 & 0 \\ \frac{sa}{2c} & 0 & 1 \end{pmatrix}$$

$$\mathbf{F}\Big|_{\boldsymbol{\beta}=\left(\frac{1}{\sqrt{2}},\frac{1}{\sqrt{2}},0\right)}^{\lambda^{\delta,2}}(s) = \omega \begin{pmatrix} 1 & \frac{s}{2} & 0 \\ \frac{s}{2} & 1 & 0 \\ 0 & 0 & 1 \end{pmatrix}.$$

$$\tag{C.6}$$

45

Appendix C.5. Orthorhombic system

For orthorhombic crystals MAELAS generates 9 sets of deformed cells using the following deformation gradients

$$
\left.\boldsymbol{F}\right|^{\lambda_1}_{\boldsymbol{\beta}=(1,0,0)}(s) = \begin{pmatrix} 1+s & 0 & 0 \\ 0 & \frac{1}{\sqrt{1+s}} & 0 \\ 0 & 0 & \frac{1}{\sqrt{1+s}} \end{pmatrix}, \left.\boldsymbol{F}\right|^{\lambda_2}_{\boldsymbol{\beta}=(1,0,0)}(s) = \begin{pmatrix} 1+s & 0 & 0 \\ 0 & \frac{1}{\sqrt{1+s}} & 0 \\ 0 & 0 & \frac{1}{\sqrt{1+s}} \end{pmatrix}
$$

$$
\left.\boldsymbol{F}\right|^{\lambda_3}_{\boldsymbol{\beta}=(0,1,0)}(s) = \begin{pmatrix} \frac{1}{\sqrt{1+s}} & 0 & 0 \\ 0 & 1+s & 0 \\ 0 & 0 & \frac{1}{\sqrt{1+s}} \end{pmatrix}, \left.\boldsymbol{F}\right|^{\lambda_4}_{\boldsymbol{\beta}=(0,1,0)}(s) = \begin{pmatrix} \frac{1}{\sqrt{1+s}} & 0 & 0 \\ 0 & 1+s & 0 \\ 0 & 0 & \frac{1}{\sqrt{1+s}} \end{pmatrix}
$$

$$
\left.\boldsymbol{F}\right|^{\lambda_5}_{\boldsymbol{\beta}=(0,0,1)}(s) = \begin{pmatrix} \frac{1}{\sqrt{1+s}} & 0 & 0 \\ 0 & \frac{1}{\sqrt{1+s}} & 0 \\ 0 & 0 & 1+s \end{pmatrix}, \left.\boldsymbol{F}\right|^{\lambda_6}_{\boldsymbol{\beta}=(0,0,1)}(s) = \begin{pmatrix} \frac{1}{\sqrt{1+s}} & 0 & 0 \\ 0 & \frac{1}{\sqrt{1+s}} & 0 \\ 0 & 0 & 1+s \end{pmatrix}
$$

$$
\left.\boldsymbol{F}\right|^{\lambda_7}_{\boldsymbol{\beta}=\frac{(a,b,0)}{\sqrt{a^2+b^2}}}(s) = \omega \begin{pmatrix} 1 & \frac{sb}{2a} & 0 \\ \frac{sa}{2b} & 1 & 0 \\ 0 & 0 & 1 \end{pmatrix}, \left.\boldsymbol{F}\right|^{\lambda_8}_{\boldsymbol{\beta}=\frac{(a,0,c)}{\sqrt{a^2+c^2}}}(s) = \omega \begin{pmatrix} 1 & 0 & \frac{sc}{2a} \\ 0 & 1 & 0 \\ \frac{sa}{2c} & 0 & 1 \end{pmatrix}
$$

$$
\left.\boldsymbol{F}\right|^{\lambda_9}_{\boldsymbol{\beta}=\frac{(0,b,c)}{\sqrt{b^2+c^2}}}(s) = \omega \begin{pmatrix} 1 & 0 & 0 \\ 0 & 1 & \frac{sc}{2b} \\ 0 & \frac{sb}{2c} & 1 \end{pmatrix}.
$$

$$(C.7)$$

References

[1] M. Gibbs, Modern trends in magnetostriction, Springer, 2001.

[2] N. Ekreem, A. Olabi, T. Prescott, A. Rafferty, M. Hashmi, An overview of magnetostriction, its use and methods to measure these properties, Journal of Materials Processing Technology 191 (1) (2007) 96 – 101, advances in Materials and Processing Technologies, July 30th - August 3rd 2006, Las Vegas, Nevada. doi:https://doi.org/10.1016/j.jmatprotec.2007.03.064. URL http://www.sciencedirect.com/science/article/pii/S0924013607002889

[3] F. T. Calkins, A. B. Flatau, M. J. Dapino, Overview of magnetostrictive sensor technology, Journal of Intelligent Material Systems and Structures 18 (10) (2007) 1057–1066. arXiv:https://doi.org/10.1177/

1045389X06072358, doi:10.1177/1045389X06072358.
URL https://doi.org/10.1177/1045389X06072358

[4] V. Apicella, C. S. Clemente, D. Davino, D. Leone, C. Visone, Review of modeling and control of magnetostrictive actuators, Actuators 8 (2). doi:10.3390/act8020045.
URL https://www.mdpi.com/2076-0825/8/2/45

[5] A. Clark, Chapter 7 magnetostrictive rare earth-Fe$_2$ compounds, Vol. 1 of Handbook of Ferromagnetic Materials, Elsevier, 1980, pp. 531 – 589. doi:https://doi.org/10.1016/S1574-9304(05)80122-1.
URL http://www.sciencedirect.com/science/article/pii/S1574930405801221

[6] G. Engdahl, Handbook of giant magnetostrictive materials, Academic Press, 1999.

[7] A. Andreev, Chapter 2 Thermal expansion anomalies and spontaneous magnetostriction in rare-earth intermetallics with cobalt and iron, Vol. 8 of Handbook of Magnetic Materials, Elsevier, 1995, pp. 59 – 187. doi:https://doi.org/10.1016/S1567-2719(05)80031-9.
URL http://www.sciencedirect.com/science/article/pii/S1567271905800319

[8] J. R. Cullen, A. E. Clark, K. B. Hathaway, Materials, science and technology, VCH Publishings, 1994, Ch. 16 - Magnetostrictive Materials, pp. 529–565.

[9] S. Massari, M. Ruberti, Rare earth elements as critical raw materials: Focus on international markets and future strategies, Resources Policy 38 (1) (2013) 36 – 43. doi:https://doi.org/10.1016/j.resourpol.2012.07.001.
URL http://www.sciencedirect.com/science/article/pii/S0301420712000530

[10] D. Fritsch, C. Ederer, First-principles calculation of magnetoelastic coefficients and magnetostriction in the spinel ferrites CoFe$_2$O$_4$ and NiFe$_2$O$_4$, Phys. Rev. B 86 (2012) 014406. doi:10.1103/PhysRevB.86.014406.
URL https://link.aps.org/doi/10.1103/PhysRevB.86.014406

[11] H. Wang, Y. N. Zhang, R. Q. Wu, L. Z. Sun, D. S. Xu, Z. D. Zhang, Understanding strong magnetostriction in Fe$_{100-x}$Ga$_x$ alloys, Scientific Reports

3 (1) (2013) 3521. `doi:10.1038/srep03521`.
URL `https://doi.org/10.1038/srep03521`

[12] M. Dapino, Encyclopedia of Smart Materials, John Wiley and Sons, Inc., New York, 2000.

[13] N. S. Akulov, Z. Physik 52, 389.

[14] R. Becker, W. Doring, Ferromagnetismus, Verlag. Julius Springer, Berlin, 1939.

[15] W. P. Mason, Derivation of magnetostriction and anisotropic energies for hexagonal, tetragonal, and orthorhombic crystals, Phys. Rev. 96 (1954) 302–310. `doi:10.1103/PhysRev.96.302`.
URL `https://link.aps.org/doi/10.1103/PhysRev.96.302`

[16] A. E. Clark, B. F. DeSavage, R. Bozorth, Anomalous Thermal Expansion and Magnetostriction of Single-Crystal Dysprosium, Phys. Rev. 138 (1965) A216–A224. `doi:10.1103/PhysRev.138.A216`.
URL `https://link.aps.org/doi/10.1103/PhysRev.138.A216`

[17] E. Callen, H. B. Callen, Magnetostriction, forced magnetostriction, and anomalous thermal expansion in ferromagnets, Phys. Rev. 139 (1965) A455–A471. `doi:10.1103/PhysRev.139.A455`.
URL `https://link.aps.org/doi/10.1103/PhysRev.139.A455`

[18] R. Wu, A. J. Freeman, First principles determinations of magnetostriction in transition metals (invited), Journal of Applied Physics 79 (8) (1996) 6209–6212. `arXiv:https://aip.scitation.org/doi/pdf/10.1063/1.362073`, `doi:10.1063/1.362073`.
URL `https://aip.scitation.org/doi/abs/10.1063/1.362073`

[19] R. Wu, L. Chen, A. Freeman, First principles determination of magnetostriction in bulk transition metals and thin films, Journal of Magnetism and Magnetic Materials 170 (1) (1997) 103 – 109. `doi:https://doi.org/10.1016/S0304-8853(97)00004-8`.
URL `http://www.sciencedirect.com/science/article/pii/S0304885397000048`

[20] R. Wu, L. Chen, A. Shick, A. Freeman, First-principles determinations of magneto-crystalline anisotropy and magnetostriction in bulk and thin-film

transition metals, Journal of Magnetism and Magnetic Materials 177-181 (1998) 1216 – 1219, international Conference on Magnetism (Part II). `doi:https://doi.org/10.1016/S0304-8853(97)00382-X`.
URL `http://www.sciencedirect.com/science/article/pii/S030488539700382X`

[21] T. Burkert, O. Eriksson, P. James, S. I. Simak, B. Johansson, L. Nordström, Calculation of uniaxial magnetic anisotropy energy of tetragonal and trigonal Fe, Co, and Ni, Phys. Rev. B 69 (2004) 104426. `doi:10.1103/PhysRevB.69.104426`.
URL `https://link.aps.org/doi/10.1103/PhysRevB.69.104426`

[22] G. Petculescu, R. Wu, R. McQueeney, Chapter three - magnetoelasticity of bcc Fe-Ga Alloys, Vol. 20 of Handbook of Magnetic Materials, Elsevier, 2012, pp. 123 – 226. `doi:https://doi.org/10.1016/B978-0-444-56371-2.00003-9`.
URL `http://www.sciencedirect.com/science/article/pii/B9780444563712000039`

[23] Y. N. Zhang, J. X. Cao, R. Q. Wu, Rigid band model for prediction of magnetostriction of iron-gallium alloys, Applied Physics Letters 96 (6) (2010) 062508. `arXiv:https://doi.org/10.1063/1.3318420`, `doi:10.1063/1.3318420`.
URL `https://doi.org/10.1063/1.3318420`

[24] Y. Zhang, R. Wu, Mechanism of large magnetostriction of galfenol, IEEE Transactions on Magnetics 47 (10) (2011) 4044–4049.

[25] Y. Zhang, H. Wang, R. Wu, First-principles determination of the rhombohedral magnetostriction of $Fe_{100-x}Al_x$ and $Fe_{100-x}Ga_x$ alloys, Phys. Rev. B 86 (2012) 224410. `doi:10.1103/PhysRevB.86.224410`.
URL `https://link.aps.org/doi/10.1103/PhysRevB.86.224410`

[26] S. C. Hong, W. S. Yun, R. Wu, Giant magnetostriction of $Fe_{1-x}Be_x$ alloy: A first-principles study, Phys. Rev. B 79 (2009) 054419. `doi:10.1103/PhysRevB.79.054419`.
URL `https://link.aps.org/doi/10.1103/PhysRevB.79.054419`

[27] V. I. Gavrilenko, R. Q. Wu, Magnetostriction and magnetism of rare earth intermetallic compounds: First principle study, Journal of Applied

Physics 89 (11) (2001) 7320–7322. arXiv:https://doi.org/10.1063/1.1356038, doi:10.1063/1.1356038.
URL https://doi.org/10.1063/1.1356038

[28] R. Wu, Magnetism and magnetostriction in $GdFe_2$ and $GdCo_2$, Journal of Applied Physics 85 (8) (1999) 6217–6219. arXiv:https://doi.org/10.1063/1.370226, doi:10.1063/1.370226.
URL https://doi.org/10.1063/1.370226

[29] M. Werwiński, W. Marciniak, Ab initio study of magnetocrystalline anisotropy, magnetostriction, and Fermi surface of $L1_0$ FeNi (tetrataenite), Journal of Physics D: Applied Physics 50 (49) (2017) 495008. doi:10.1088/1361-6463/aa958a.
URL https://doi.org/10.1088/1361-6463/aa958a

[30] E. Wasserman, Chapter 3 Invar: Moment-volume instabilities in transition metals and alloys, Vol. 5 of Handbook of Ferromagnetic Materials, Elsevier, 1990, pp. 237 – 322. doi:https://doi.org/10.1016/S1574-9304(05)80063-X.
URL http://www.sciencedirect.com/science/article/pii/S157493040580063X

[31] R. Skomski, J. M. D. Coey, Permanent magnetism, Institute of Physics Publishing, 1999.

[32] J. Joule, On a new class of magnetic forces, Annals of Electricity, Magnetism, and Chemistry 8 (1842) 219–224.

[33] L. D. Landau, E. M. Lifshitz, Theory of elasticity / by L. D. Landau and E. M. Lifshitz ; translated from the Russian by J. B. Sykes and W. H. Reid, Pergamon London, 1959.

[34] R. Birss, The saturation magnetostriction of ferromagnetics, Advances in Physics 8 (31) (1959) 252–291. arXiv:https://doi.org/10.1080/00018735900101198, doi:10.1080/00018735900101198.
URL https://doi.org/10.1080/00018735900101198

[35] C. Kittel, Physical theory of ferromagnetic domains, Rev. Mod. Phys. 21 (1949) 541–583. doi:10.1103/RevModPhys.21.541.
URL https://link.aps.org/doi/10.1103/RevModPhys.21.541

[36] H. Mueller, Properties of rochelle salt. iv, Phys. Rev. 58 (1940) 805–811. `doi:10.1103/PhysRev.58.805`.
URL `https://link.aps.org/doi/10.1103/PhysRev.58.805`

[37] D. C. Wallace, Thermodynamics of Crystals, Wiley, New York, 1972.

[38] F. Mouhat, F. m. c.-X. Coudert, Necessary and sufficient elastic stability conditions in various crystal systems, Phys. Rev. B 90 (2014) 224104. `doi:10.1103/PhysRevB.90.224104`.
URL `https://link.aps.org/doi/10.1103/PhysRevB.90.224104`

[39] L. A.E.H., A Treatise on the Mathematical Theory of Elasticity, Dover publisher, New York, 1944.

[40] R. C. O'Handley, Modern magnetic materials, Wiley, 2000.

[41] E. W. Lee, Magnetostriction and magnetomechanical effects, Reports on Progress in Physics 18 (1) (1955) 184–229. `doi:10.1088/0034-4885/18/1/305`.

[42] A. Reuss, Berechnung der Fließgrenze von Mischkristallen auf Grund der Plastizitätsbedingung für Einkristalle, ZAMM - Journal of Applied Mathematics and Mechanics 9 (1) (1929) 49–58. `arXiv:https://onlinelibrary.wiley.com/doi/pdf/10.1002/zamm.19290090104`, `doi:10.1002/zamm.19290090104`.
URL `https://onlinelibrary.wiley.com/doi/abs/10.1002/zamm.19290090104`

[43] R. Hill, The elastic behaviour of a crystalline aggregate, Proceedings of the Physical Society. Section A 65 (5) (1952) 349–354. `doi:10.1088/0370-1298/65/5/307`.

[44] S. Zhang, R. Zhang, AELAS: Automatic ELAStic property derivations via high-throughput first-principles computation, Computer Physics Communications 220 (2017) 403 – 416. `doi:https://doi.org/10.1016/j.cpc.2017.07.020`.
URL `http://www.sciencedirect.com/science/article/pii/S0010465517302400`

[45] E. du Trémolet de Lacheisserie, D. Gignoux, M. Schlenker, Magnetism, Springer New York, New York, NY, 2002, Ch. 12 Magnetoelastic Effects, pp. 351–398.

[46] W. J. Carr, Chapter 10 Magnetostriction, Magnetic properties of metals and alloys, American Society for Metals, Cleveland, 1959.

[47] G. Kresse, J. Hafner, Ab initio molecular dynamics for liquid metals, Phys. Rev. B 47 (1993) 558–561. doi:10.1103/PhysRevB.47.558.
URL https://link.aps.org/doi/10.1103/PhysRevB.47.558

[48] G. Kresse, J. Furthmüller, Efficiency of ab-initio total energy calculations for metals and semiconductors using a plane-wave basis set, Computational Materials Science 6 (1) (1996) 15 – 50. doi:https://doi.org/10.1016/0927-0256(96)00008-0.
URL http://www.sciencedirect.com/science/article/pii/0927025696000080

[49] G. Kresse, J. Furthmüller, Efficient iterative schemes for ab initio total-energy calculations using a plane-wave basis set, Phys. Rev. B 54 (1996) 11169–11186. doi:10.1103/PhysRevB.54.11169.
URL https://link.aps.org/doi/10.1103/PhysRevB.54.11169

[50] S. P. Ong, W. D. Richards, A. Jain, G. Hautier, M. Kocher, S. Cholia, D. Gunter, V. L. Chevrier, K. A. Persson, G. Ceder, Python materials genomics (pymatgen): A robust, open-source python library for materials analysis, Computational Materials Science 68 (2013) 314 – 319. doi:https://doi.org/10.1016/j.commatsci.2012.10.028.
URL http://www.sciencedirect.com/science/article/pii/S0927025612006295

[51] P. Nieves, S. Arapan, A. P. Kądzielawa, D. Legut, MAELASviewer: An online tool to visualize magnetostriction, Sensors 20 (22). doi:10.3390/s20226436.
URL https://www.mdpi.com/1424-8220/20/22/6436

[52] https://maelasviewer.herokuapp.com.

[53] https://github.com/pnieves2019/MAELASwiewer.

[54] https://github.com/pnieves2019/MAELAS.

[55] G. Kresse, D. Joubert, From ultrasoft pseudopotentials to the projector augmented-wave method, Phys. Rev. B 59 (1999) 1758–1775. `doi:10.1103/PhysRevB.59.1758`.
URL `https://link.aps.org/doi/10.1103/PhysRevB.59.1758`

[56] J. P. Perdew, K. Burke, M. Ernzerhof, Generalized gradient approximation made simple, Phys. Rev. Lett. 77 (1996) 3865–3868. `doi:10.1103/PhysRevLett.77.3865`.
URL `https://link.aps.org/doi/10.1103/PhysRevLett.77.3865`

[57] D. Hobbs, G. Kresse, J. Hafner, Fully unconstrained noncollinear magnetism within the projector augmented-wave method, Phys. Rev. B 62 (2000) 11556–11570. `doi:10.1103/PhysRevB.62.11556`.
URL `https://link.aps.org/doi/10.1103/PhysRevB.62.11556`

[58] H. J. Monkhorst, J. D. Pack, Special points for brillouin-zone integrations, Phys. Rev. B 13 (1976) 5188–5192. `doi:10.1103/PhysRevB.13.5188`.
URL `https://link.aps.org/doi/10.1103/PhysRevB.13.5188`

[59] P. Nieves, J. Tranchida, S. Arapan, D. Legut, Spin-lattice model for cubic crystals (2020). `arXiv:2012.05076`.

[60] J. Tranchida, S. Plimpton, P. Thibaudeau, A. Thompson, Massively parallel symplectic algorithm for coupled magnetic spin dynamics and molecular dynamics, Journal of Computational Physics 372 (2018) 406 – 425. `doi:https://doi.org/10.1016/j.jcp.2018.06.042`.
URL `http://www.sciencedirect.com/science/article/pii/S0021999118304200`

[61] S. Plimpton, Fast parallel algorithms for short-range molecular dynamics, Journal of Computational Physics 117 (1) (1995) 1 – 19. `doi:https://doi.org/10.1006/jcph.1995.1039`.
URL `http://www.sciencedirect.com/science/article/pii/S002199918571039X`

[62] M. Getzlaff, Fundamentals of magnetism, Springer, Berlin, Heidelberg, 2008.

[63] A. Hubert, W. Unger, J. Kranz, Messung der magnetostriktionskonstanten des kobalts als funktion der temperatur, Z. Physik 224 (1) (1969) 148–155.

doi:10.1007/BF01392243.
URL https://doi.org/10.1007/BF01392243

[64] M. C. Nguyen, Y. Yao, C.-Z. Wang, K.-M. Ho, V. P. Antropov, Magnetocrystalline anisotropy in cobalt based magnets: a choice of correlation parameters and the relativistic effects, Journal of Physics: Condensed Matter 30 (19) (2018) 195801. doi:10.1088/1361-648x/aab9fa.
URL https://doi.org/10.1088/1361-648X/aab9fa

[65] H. Shima, K. Oikawa, A. Fujita, K. Fukamichi, K. Ishida, A. Sakuma, Lattice axial ratio and large uniaxial magnetocrystalline anisotropy in L1$_0$-type FePd single crystals prepared under compressive stress, Phys. Rev. B 70 (2004) 224408. doi:10.1103/PhysRevB.70.224408.
URL https://link.aps.org/doi/10.1103/PhysRevB.70.224408

[66] H. Shima, K. Oikawa, A. Fujita, K. Fukamichi, K. Ishida, Magnetic anisotropy and mangnetostriction in L1$_0$ FePd alloy, Journal of Magnetism and Magnetic Materials 272-276 (2004) 2173 – 2174, proceedings of the International Conference on Magnetism (ICM 2003). doi:https://doi.org/10.1016/j.jmmm.2003.12.898.
URL http://www.sciencedirect.com/science/article/pii/S0304885303018316

[67] M. de Jong, W. Chen, T. Angsten, A. Jain, R. Notestine, A. Gamst, M. Sluiter, C. Krishna Ande, S. van der Zwaag, J. J. Plata, C. Toher, S. Curtarolo, G. Ceder, K. A. Persson, M. Asta, Charting the complete elastic properties of inorganic crystalline compounds, Scientific Data 2 (1) (2015) 150009. doi:10.1038/sdata.2015.9.
URL https://doi.org/10.1038/sdata.2015.9

[68] A. Jain, S. Ong, G. Hautier, W. Chen, W. Richards, S. Dacek, S. Cholia, D. Gunter, D. Skinner, G. Ceder, K. Persson, The materials project: A materials genome approach to accelerating materials innovation, APL Materials 1 (2013) 011002.

[69] K. Persson, Materials data on Fe (SG:229) by materials project (1 2015). doi:10.17188/1189317.

[70] J. A. Rayne, B. S. Chandrasekhar, Elastic constants of iron from 4.2 to 300 k, Phys. Rev. 122 (1961) 1714–1716. doi:10.1103/PhysRev.122.1714.
URL https://link.aps.org/doi/10.1103/PhysRev.122.1714

[71] K. Persson, Materials data on Co (SG:194) by materials project (2 2016). doi:10.17188/1263614.

[72] H. J. McSkimin, Measurement of the elastic constants of single crystal cobalt, Journal of Applied Physics 26 (4) (1955) 406–409. arXiv:https://doi.org/10.1063/1.1722007, doi:10.1063/1.1722007.
URL https://doi.org/10.1063/1.1722007

[73] K. Persson, Materials data on YCo5 (SG:191) by materials project (2 2016). doi:10.17188/1202401.

[74] K. Persson, Materials data on Ni (SG:225) by materials project (2 2016). doi:10.17188/1199153.

[75] B.-J. Lee, J.-H. Shim, M. I. Baskes, Semiempirical atomic potentials for the fcc metals Cu, Ag, Au, Ni, Pd, Pt, Al, and Pb based on first and second nearest-neighbor modified embedded atom method, Phys. Rev. B 68 (2003) 144112. doi:10.1103/PhysRevB.68.144112.
URL https://link.aps.org/doi/10.1103/PhysRevB.68.144112

[76] K. Persson, Materials data on Fe2Si (SG:164) by materials project (2 2016). doi:10.17188/1198977.

[77] K. Persson, Materials data on FePd (SG:123) by materials project (2 2016). doi:10.17188/1202438.

[78] A. Al-Ghaferi, P. Müllner, H. Heinrich, G. Kostorz, J. Wiezorek, Elastic constants of equiatomic $L1_0$-ordered FePd single crystals, Acta Materialia 54 (4) (2006) 881 – 889. doi:https://doi.org/10.1016/j.actamat.2005.10.018.
URL http://www.sciencedirect.com/science/article/pii/S1359645405006129

[79] K. Persson, Materials data on YCo (SG:63) by materials project (2 2016). doi:10.17188/1307912.

[80] J. Kübler, Theory of itinerant electron magnetism, Oxford University Press, New York, 2009.

[81] S. V. Halilov, A. Y. Perlov, P. M. Oppeneer, A. N. Yaresko, V. N. Antonov, Magnetocrystalline anisotropy energy in cubic fe, co, and ni: Applicability

of local-spin-density theory reexamined, Phys. Rev. B 57 (1998) 9557–9560.
`doi:10.1103/PhysRevB.57.9557`.
URL `https://link.aps.org/doi/10.1103/PhysRevB.57.9557`

[82] J. Trygg, B. Johansson, O. Eriksson, J. M. Wills, Total energy calculation of the magnetocrystalline anisotropy energy in the ferromagnetic 3d metals, Phys. Rev. Lett. 75 (1995) 2871–2874. `doi:10.1103/PhysRevLett.75.2871`.
URL `https://link.aps.org/doi/10.1103/PhysRevLett.75.2871`

[83] M. Fähnle, M. Komelj, R. Q. Wu, G. Y. Guo, Magnetoelasticity of Fe: Possible failure of ab initio electron theory with the local-spin-density approximation and with the generalized-gradient approximation, Phys. Rev. B 65 (2002) 144436. `doi:10.1103/PhysRevB.65.144436`.
URL `https://link.aps.org/doi/10.1103/PhysRevB.65.144436`

[84] N. J. Jones, G. Petculescu, M. Wun-Fogle, J. B. Restorff, A. E. Clark, K. B. Hathaway, D. Schlagel, T. A. Lograsso, Rhombohedral magnetostriction in dilute iron (Co) alloys, Journal of Applied Physics 117 (17) (2015) 17A913. `arXiv:https://doi.org/10.1063/1.4916541`, `doi:10.1063/1.4916541`.
URL `https://doi.org/10.1063/1.4916541`

[85] M. Fähnle, M. Komelj, R. Q. Wu, G. Y. Guo, Magnetoelasticity of fe: Possible failure of ab initio electron theory with the local-spin-density approximation and with the generalized-gradient approximation, Phys. Rev. B 65 (2002) 144436. `doi:10.1103/PhysRevB.65.144436`.
URL `https://link.aps.org/doi/10.1103/PhysRevB.65.144436`

[86] J. Sun, A. Ruzsinszky, J. P. Perdew, Strongly constrained and appropriately normed semilocal density functional, Phys. Rev. Lett. 115 (2015) 036402. `doi:10.1103/PhysRevLett.115.036402`.
URL `https://link.aps.org/doi/10.1103/PhysRevLett.115.036402`

[87] A. I. Liechtenstein, V. I. Anisimov, J. Zaanen, Density-functional theory and strong interactions: Orbital ordering in Mott-Hubbard insulators, Phys. Rev. B 52 (1995) R5467–R5470. `doi:10.1103/PhysRevB.52.R5467`.
URL `https://link.aps.org/doi/10.1103/PhysRevB.52.R5467`

[88] A. Mishima, H. Fujii, T. Okamoto, Anomalous Saturation Magnetostriction of Gd Single Crystal, Journal of the Physical Society of Japan 40 (4) (1976) 962–967. arXiv:https://doi.org/10.1143/JPSJ.40.962, doi:10.1143/JPSJ.40.962.
URL https://doi.org/10.1143/JPSJ.40.962

[89] S. L. Dudarev, G. A. Botton, S. Y. Savrasov, C. J. Humphreys, A. P. Sutton, Electron-energy-loss spectra and the structural stability of nickel oxide: An lsda+u study, Phys. Rev. B 57 (1998) 1505–1509. doi:10.1103/PhysRevB.57.1505.
URL https://link.aps.org/doi/10.1103/PhysRevB.57.1505

[90] H. Kudielka, Die Kristallstruktur von Fe_2Si, ihre Verwandtschaft zu den Ordnungsstrukturen des α-(Fe,Si)-Mischkristalls und zur Fe_5Si_3-Struktur, Zeitschrift für Kristallographie - Crystalline Materials 145 (1-6) (01 Dec. 1977) 177 – 189. doi:https://doi.org/10.1524/zkri.1977.145.16.177.
URL https://www.degruyter.com/view/journals/zkri/145/1-6/article-p177.xml

[91] Y. Sun, Z. Zhuo, X. Wu, J. Yang, Room-temperature ferromagnetism in two-dimensional Fe_2Si nanosheet with enhanced spin-polarization ratio, Nano Letters 17 (5) (2017) 2771–2777. doi:10.1021/acs.nanolett.6b04884.
URL https://doi.org/10.1021/acs.nanolett.6b04884

[92] A. V. Krukau, O. A. Vydrov, A. F. Izmaylov, G. E. Scuseria, Influence of the exchange screening parameter on the performance of screened hybrid functionals, The Journal of Chemical Physics 125 (22) (2006) 224106. arXiv:https://doi.org/10.1063/1.2404663, doi:10.1063/1.2404663.
URL https://doi.org/10.1063/1.2404663

[93] C. P. Tang, K. V. Tam, S. J. Xiong, J. Cao, X. Zhang, The structure and electronic properties of hexagonal Fe_2Si, AIP Advances 6 (6) (2016) 065317. arXiv:https://doi.org/10.1063/1.4954667, doi:10.1063/1.4954667.
URL https://doi.org/10.1063/1.4954667

[94] T. Hikosaka, F. Nakamura, S. Oikawa, A. Takeo, Y. Tanaka, Low noise FeAlSi soft magnetic under-layer for CoPtCrO double-layered perpendicular recording media, IEEE Transactions on Magnetics 37 (4) (2001) 1586–1588.

[95] P. Villars, K. Cenzual, R. Gladyshevskii, Handbook, De Gruyter, Berlin, Boston, 27 Nov. 2015. `doi:https://doi.org/10.1515/9783110334678`. URL `https://www.degruyter.com/view/title/304631`

[96] W. P. Mason, A phenomenological derivation of the first- and second-order magnetostriction and morphic effects for a nickel crystal, Phys. Rev. 82 (1951) 715–723. `doi:10.1103/PhysRev.82.715`. URL `https://link.aps.org/doi/10.1103/PhysRev.82.715`

[97] E. B. Tadmor, R. E. Miller, Modeling Materials, Cambridge University Press, 2009. `doi:10.1017/cbo9781139003582`. URL `https://doi.org/10.1017/cbo9781139003582`

[98] G. Guo, Orientation dependence of the magnetoelastic coupling constants in strained FCC Co and Ni: an ab initio study, Journal of Magnetism and Magnetic Materials 209 (1) (2000) 33 – 36. `doi:https://doi.org/10.1016/S0304-8853(99)00639-3`. URL `http://www.sciencedirect.com/science/article/pii/S0304885399006393`